

# Fast and Accurate Computation Tools for Gravitational Waveforms from Binary Stars with any Orbital Eccentricity

V. Pierro <sup>1</sup>, I.M. Pinto <sup>1</sup>, A.D. Spallicci <sup>1</sup>, E. Laserra <sup>2</sup>, F. Recano <sup>2</sup>.

<sup>1</sup>*Waves Group, Univ. of Sannio at Benevento, Italy*

<sup>2</sup>*D.I.I.M.A., Univ. of Salerno, Italy*

27 October 2018

**Keywords:** gravitational waves, binary stars, computational techniques, data analysis, mathematical methods, space detectors.

## ABSTRACT

The relevance of orbital eccentricity in the detection of gravitational radiation from (steady-state) binary stars is emphasized. Computationally effective (fast and accurate) tools for constructing gravitational wave templates from binary stars with any orbital eccentricity are introduced, including tight estimation criteria of the pertinent truncation and approximation errors.

## 1 INTRODUCTION

Gravitational wave detection experiments in space, including satellite Doppler-Tracking (Bertotti and Iess, 1999) and LISA (<http://lisa.jpl.nasa.gov>), will hopefully open a window on the low-frequency part of the gravitational wave (henceforth GW) spectrum of cosmic origin. In these frequency bands, binary stars are among the most promising continuous detectable source.

A substantial fraction of binaries are expected to have orbits with *non negligible eccentricity* (Barone et al., 1988; Hils et al., 1992; Pierro and Pinto, 1996c) resulting into the emission of *several harmonics* of the fundamental orbital frequency. The importance of this fact from the standpoint of signal detection and estimation has been already noted.

For *coalescing binaries*, Pierro and Pinto (1996b) and Martel and Poisson (1999) pointed out that neglecting residual (albeit very small) orbital eccentricities may seriously deteriorate matched-filter detection performance. Their results, obtained in the frame of the simplest (newtonian) Peters Mathews (henceforth PM) model (Peters and Mathews, 1963; Peters 1964; Pierro and Pinto 1996c), support the *qualitative* conclusion that residual orbital eccentricities cannot be *bona fide* disregarded in building templates for matched-filter detection of gravitational wave chirps from inspiraling binaries<sup>\*</sup>.

For *steady-state* binaries with non-zero orbital eccentricity, on the other hand, using circular-orbit waveform templates, i.e. neglecting higher order harmonics, implies a *potentially large* loss of signal-to-noise ratio (henceforth SNR), leading to significantly worse detector’s performance, as will be shown in the sequel.

The main goals of the present paper are:

- i) to provide some quantitative hint for validating the applicability of the simple PM model to steady-state binaries;
- ii) to gauge the loss in SNR due to the simple circular-orbit assumption and, more generally, to set some criteria for spectral waveform truncation;
- iii) to introduce *efficient* (accurate and fast) computational tools for constructing gravitational waveform templates for (steady-state) binary sources with *any* orbital eccentricity.

The paper is organized as follows. In *Sect. 2* we introduce some (dimensionless) parameters whereby the applicability of the PM model to specific sources can be assessed. In *Sect.s 3a* and *3b* we review the GW spectra and waveforms in the frame of the PM model. In *Sect.s 4a* and *4b* we show how to evaluate the total harmonic distortion due to spectral waveform

<sup>\*</sup> The effect of a residual (tiny) orbital eccentricity on the radiation emitted from an *inspiraling* binary system was also considered in (Moreno et al., 1994), with special emphasis on the possible relevance of periastron advance. The results in (Moreno et al., 1994) are unfortunately affected by several errors and misprints.

truncation, and introduce a modified Carlini Meissel expansion tool for fast and accurate GW harmonics computation. The results in this section can be readily extended, in principle, to higher-order post-newtonian (henceforth PN) models. As an application, in *Sect. 5* we apply our formalism to some paradigm eccentric binary sources. Conclusions follow under *Sect. 6*. Technical developments are collected in *Appendix A* to *C*.

## 2 STEADY-STATE BINARIES: THE PETERS-MATHEWS MODEL

The PM model for gravitational wave emission from binary systems in a Keplerian orbit was introduced in the sixties (Peters and Mathews, 1963, Peters 1964), and recently re-examined (Pierro and Pinto, 1996a). It relies on the following main assumptions: i) point mass, ii) weak field, iii) slow motion, and iv) adiabatic evolution (negligible change of the orbital parameters over each orbit). These conditions can be checked in terms of the following inequalities (Pierro and Pinto, 1996a):

$$\xi_1 := \frac{\text{source gravitational radius}}{\text{aphastral separation}} = 2\chi^{-2/3}(1-e)^{-1} \ll 1, \quad (1)$$

$$\xi_2 := \frac{\text{aphastral velocity}}{\text{velocity of light}} = \chi^{-1/3} \left( \frac{1+e}{1-e} \right)^{1/2} \ll 1, \quad (2)$$

$$\xi_3 := \sup \left\{ \left| \frac{dT}{dt} \right|, \left| e^{-1} \frac{de}{dt} T \right| \right\} = \frac{152\pi}{15} (1-\Delta^2) \chi^{-5/3} \cdot \left( 1 + \frac{121}{304} e^2 \right) (1-e^2)^{-5/2} \ll 1, \quad (3)$$

where as already stated  $\chi = cT/\pi r_g$ ,  $T$  being the orbital period,  $r_g = 2G(M_1 + M_2)/c^2$  is the source gravitational radius,  $M_{1,2}$  are the companion masses,  $\Delta = |M_1 - M_2|/(M_1 + M_2)$  and  $e$  is the eccentricity.

Tidal effects could be neglected provided neither companion star fills its Roche lobe. Following Eggleton (1983), this translates into:

$$\xi_1 \ll \Lambda^{-1} \frac{2}{1+\Delta} \left\{ 0.6 + \left( \frac{1-\Delta}{1+\Delta} \right)^{2/3} \ln \left[ 1 + \left( \frac{1-\Delta}{1+\Delta} \right)^{-1/3} \right] \right\}^{-1}, \quad (4)$$

where  $\Lambda$  is the ratio between the physical and gravitational companion radius<sup>†</sup>.

For most steady-state binary systems, i.e. long before coalescence,  $\xi_1$  to  $\xi_3$  above are fairly small (see e.g. *Sect. 5*), and the PM model turns out to be perfectly adequate.

## 3A STEADY-STATE BINARIES: SPECTRA

According to the PM model, the GW power  $\overline{\mathcal{L}}_n^{+, \times}$  radiated at the  $n^{\text{th}}$  harmonic of the orbital frequency by a steady binary source can be conveniently cast into the following universal form (Barone et al., 1988):

$$\overline{\mathcal{L}}_n^{+, \times} = \frac{2G}{5c^5} \chi^{-10/3} (1-\Delta^2)^2 G_{max}(e) \overline{g}^{+, \times}(n, e) \quad (5)$$

where the superscripts  $+, \times$  refer to the fundamental GW polarization states. The spectral power distribution is embodied in the *universal* dimensionless functions  $\overline{g}^{+, \times}(n, e)$  shown in *fig.s 1.1-1.10* for  $e = 0(0.1)0.9$ . For circular orbits ( $e = 0$ ) only the second harmonic is emitted. The function  $G_{max}(e)$  plotted in *fig. 2* is the ratio between the total luminosity (sum over both polarizations) of the brightest GW spectral line, and the total luminosity of a circular-orbit binary having the same  $\chi$  and  $\Delta$ . The brightest spectral line is the  $N_{max}$ -th harmonic of the orbital frequency, where  $N_{max}$  is a function of  $e$  only, displayed in *fig. 3*.

It is seen that for non circular orbits, *several* spectral lines with *comparable* intensities are emitted. Thus, use of the circular orbit waveform templates implies a potentially sizeable loss in the available signal power and hence in the SNR, which can spoil the detector's performance.

## 3b WAVEFORMS

The far-field metric deviation (TT gauge) in the PM model is<sup>‡</sup>:

<sup>†</sup> Typical values of  $\Lambda$  range from  $10^4$  for white dwarfs down to 3 for hadronic stars. Further departures from the standard model are expected due to the possible occurrence of mass-transfer phenomena, which would be present in closely-orbiting classical stars, as well as in binaries where one companion is an accreting collapsed object.

<sup>‡</sup> The GW field can also be obtained by inverting the Keplerian integral of motion relating time to the true anomaly, and exploiting the simple dependance of the radiated waveforms on this latter (Wahlquist, 1987). The referred procedure is purely numerical and, to the best of our knowledge, its generalization to higher PN order models is not immediate.

$$h_{\times} = \frac{\cos \vartheta}{\sqrt{2}} [2h_{xy} \cos 2\varphi - (h_{xx} - h_{yy}) \sin 2\varphi], \quad (6)$$

$$h_{+} = \frac{1}{\sqrt{2}} \left\{ \frac{3 + \cos 2\vartheta}{4} [2h_{xy} \sin 2\varphi + (h_{xx} - h_{yy}) \cos 2\varphi] - \frac{1 - \cos 2\vartheta}{4} (h_{xx} + h_{yy}) \right\}, \quad (7)$$

where the coordinates  $\vartheta$  and  $\varphi$  specify the direction of the observer in a spherical polar system where the orbit lies in the equatorial plane and the binary center of mass is at the origin.

The metric components in (6), (7) can be expanded into Fourier series under the *adiabatic assumption* that the orbital parameters *do not* change appreciably over each orbit. Hence<sup>§</sup>:

$$h_{xy} = \sum_{n=1}^{\infty} h_{xy}^{(n)} \sin \left( n \frac{2\pi}{T} t \right), \quad (8)$$

$$h_{x\pm y} = \sum_{n=1}^{\infty} h_{x\pm y}^{(n)} \cos \left( n \frac{2\pi}{T} t \right), \quad (9)$$

where  $h_{x\pm y}$  is a shorthand for  $h_{xx} \pm h_{yy}$  (see *Appendix A*),

$$h_{xy}^{(n)} = h_0 n (1 - e^2)^{1/2} [J_{n-2}(ne) + J_{n+2}(ne) - 2J_n(ne)], \quad (10)$$

$$h_{x-y}^{(n)} = 2h_0 n \{J_{n-2}(ne) - J_{n+2}(ne) - 2e [J_{n-1}(ne) - J_{n+1}(ne)] + (2/n)J_n(ne)\}, \quad (11)$$

$$h_{x+y}^{(n)} = -4h_0 J_n(ne), \quad (12)$$

and<sup>¶</sup>

$$h_0 = \frac{cT}{4\pi r} \frac{1 - \Delta^2}{\chi^{5/3}}. \quad (13)$$

For circular orbits one has simply:

$$h_{x-y}^{(n)} = 2h_{xy}^{(n)} = 4h_0 \delta_{n2}, \quad h_{x+y}^{(n)} = 0, \quad (14)$$

where  $\delta_{pq}$  is the Kronecker symbol.

For *steady state* binaries the (Robertson) periastron advance<sup>||</sup> does not produce sensible effects on the waveforms, and is thus deliberately ignored. Inclusion of the periastron advance amounts to splitting each GW spectral line into a doublet at  $\sim (2\pi/T)(1 \pm 6\chi^{-2/3})$ , which *cannot* be resolved unless the signal is Fourier-transformed over a timespan  $\sim \chi^{2/3}T$  sec. This time is, e.g.,  $\sim 5 \cdot 10^5$  years and  $\sim 2.8 \cdot 10^5$  years for *PSR1534 + 12* and *PSR1913 + 16*, respectively.

#### 4A SPECTRAL TRUNCATION AND APPROXIMATION ERROR

In order to discuss the effect of spectral truncation of (8) and (9) on the available SNR it is convenient to introduce the total harmonic distortion (henceforth THD):

$$THD = \frac{\|h - \tilde{h}\|}{\|h\|} = \left( \frac{\sum_{n=1}^{\infty} \left( h^{(n)} - \tilde{h}^{(n)} \right)^2}{\sum_{n=1}^{\infty} |h^{(n)}|^2} \right)^{1/2}, \quad (15)$$

where  $h, \tilde{h}$  represent the *exact* and *approximate* values of the metric tensor,  $h^{(n)}, \tilde{h}^{(n)}$  are the Fourier coefficients of  $h, \tilde{h}$ , respectively, and the  $L^2$ -norms are computed by taking the time average over one orbital period of the square of the argument, within the spirit of the adiabatic approximation. If only  $N_T$  harmonics are included, then

<sup>§</sup> The unknown irrelevant phase at  $t = 0$  has been set to zero.

<sup>¶</sup> Note that for  $n = 1$  eq.s (10) and (11) contain Bessel functions of order  $-1$ , for which  $J_{-1}(x) = -J_1(x)$ .

<sup>||</sup> The relativistic periastron advance was heuristically (i.e., inconsistently, from the post-newtonian expansion view point) included in (Moreno et al., 1995).

$$\tilde{h}^{(n)} = \begin{cases} h^{(n)}, & n \leq N_T, \\ 0, & n > N_T \end{cases}, \quad THD = \left( 1 - \frac{\sum_{n=1}^{N_T} |h^{(n)}|^2}{\sum_{n=1}^{\infty} |h^{(n)}|^2} \right)^{1/2}. \quad (16)$$

It is readily recognized that  $THD^2$  represents the fraction of signal power which is *lost* as an effect of truncation<sup>\*\*</sup>.

In the most general case, where besides spectral truncation, the Fourier coefficients are computed in *approximate* form (as e.g. in the next subsection), one has:

$$THD = \left( 1 - \frac{2 \sum_{n=1}^{NT} h^{(n)} \tilde{h}^{(n)} - \sum_{n=1}^{NT} |\tilde{h}^{(n)}|^2}{\sum_{n=1}^{\infty} |h^{(n)}|^2} \right)^{1/2}, \quad (17)$$

The harmonic distortions  $THD_{x\pm y}$ ,  $THD_{xy}$  due to the spectral truncation of (8), (9) can be computed for any given  $N_T$  using Kapteyn's theory (Watson, 1966, ch. 17) to evaluate in closed form the infinite sums in (17). After some lengthy but simple algebra, one obtains (see Appendix B):

$$\|h_{x+y}\|^2 = \sum_{n=1}^{\infty} |h_{x+y}^{(n)}|^2 = 8 \left[ (1 - e^2)^{-1/2} - 1 \right], \quad (18)$$

$$\|h_{x-y}\|^2 = \sum_{n=1}^{\infty} |h_{x-y}^{(n)}|^2 = e^{-4} \left\{ 4 (1 - e^2)^{-1/2} (8 - 12 e^2 + 9 e^4) - 8 (e^2 - 2)^2 \right\}, \quad (19)$$

$$\|h_{xy}\|^2 = \sum_{n=1}^{\infty} |h_{xy}^{(n)}|^2 = e^{-2} (1 - e^2)^{-1/2} \left\{ 12 + e^2 + 8 e^{-2} \left[ (1 - e^2)^{3/2} - 1 \right] \right\}, \quad (20)$$

The corresponding harmonic distortions for the  $TT$  metric components  $h_+$ ,  $h_{\times}$  can be conveniently written as follows:

$$THD_{\times} = \left\{ \left[ 4THD_{xy}^2 \|h_{xy}\|^2 \cos^2 2\varphi + THD_{x-y}^2 \|h_{x-y}\|^2 \sin^2 2\varphi \right] \cdot \left[ 4\|h_{xy}\|^2 \cos^2 2\varphi + \|h_{x-y}\|^2 \sin^2 2\varphi \right]^{-1} \right\}^{1/2}, \quad (21)$$

and:

$$\begin{aligned} THD_+ = & \left\{ \left[ (3 + \cos 2\vartheta)^2 (4THD_{xy}^2 \|h_{xy}\|^2 \sin^2 2\varphi + THD_{x-y}^2 \|h_{x-y}\|^2 \cos^2 2\varphi) + (1 - \cos 2\vartheta)^2 THD_{x+y}^2 \|h_{x+y}\|^2 + \right. \right. \\ & + 2(1 - \cos 2\vartheta)(3 + \cos 2\vartheta) \cos 2\varphi \left\langle (h_{x-y} - \tilde{h}_{x-y}), (h_{x+y} - \tilde{h}_{x+y}) \right\rangle \left. \right] \cdot \left[ (3 + \cos 2\vartheta)^2 (4\|h_{xy}\|^2 \sin^2 2\varphi + \|h_{x-y}\|^2 \cos^2 2\varphi) + \right. \\ & \left. + (1 - \cos 2\vartheta)^2 \|h_{x+y}\|^2 + 2(1 - \cos 2\vartheta)(3 + \cos 2\vartheta) \cos 2\varphi \left\langle h_{x-y}, h_{x+y} \right\rangle \right]^{-1} \right\}^{1/2}, \quad (22) \end{aligned}$$

where  $\langle \cdot, \cdot \rangle$  is the scalar product in  $L^2_{[0,T]}$ . In order to evaluate (22) the further infinite sum:

$$\langle h_{x-y}, h_{x+y} \rangle = \sum_{n=1}^{\infty} h_{x-y}^{(n)} h_{x+y}^{(n)} = -8 (1 - e^2)^{-1/2} \left\{ 1 + (1 - 2 e^{-2}) \left[ 1 - (1 - e^2)^{1/2} \right] \right\}. \quad (23)$$

is needed, which is also readily obtained as explained in Appendix B.

The harmonic distortions (21) and (22) can be sensible even at very low eccentricities ( $e \leq .1$ ). Expanding (21) and (22) to lowest order in  $e$  yields:

$$THD_{\times} = \frac{3\sqrt{10}}{4} e + \mathcal{O}(e^3), \quad (24)$$

$$THD_+ = \frac{\sqrt{4(1 - \cos 2\varphi)^2 + 12(1 - \cos 2\varphi)(3 + \cos 2\varphi) \cos 2\vartheta + 90(3 + \cos 2\varphi)^2}}{4(3 + \cos 2\varphi)} e + \mathcal{O}(e^3). \quad (25)$$

<sup>\*\*</sup> The THD is closely related to the fitting factor FF (Apostolatos, 1996) between the exact and spectral-truncated (template) waveform. From the very definitions one gets:

$$FF \sim 1 - \frac{THD^2}{2} + \mathcal{O}(THD^3).$$

The above simple expressions are fairly accurate for  $e \leq .1$ , as seen, e.g., from *fig. 4*, where the angular averages of the approximate and exact harmonic distortion are drawn, and seen to be almost indistinguishable and non-negligible. The  $(\vartheta, \varphi)$ -dependent factor in (25) is plotted in *fig. 5*. Its average value over the sphere is exactly equal to the  $(\vartheta, \varphi)$ -independent factor in (24).

The obvious question is how many terms should be included in (8) and (9) so as to keep both  $THD_+$  and  $THD_\times$  below some specified level, for any  $(\vartheta, \varphi)$ .

To answer this question one may resort to the following inequalities:

$$\max_{(\vartheta, \varphi)} THD_\times \leq \max(THD_{xy}, THD_{x-y}), \quad \max_{(\vartheta, \varphi)} THD_+ \leq \max(THD_{xy}, THD_{x-y}, THD_{x+y}) \max_{(\vartheta, \varphi)} [Q(\vartheta, \varphi, e)]. \quad (26)$$

where:

$$\begin{aligned} Q(\vartheta, \varphi, e) = & \left\{ \left[ (3 + \cos 2\vartheta)^2 (4\|h_{xy}\|^2 \sin^2 2\varphi + \|h_{x-y}\|^2 \cos^2 2\varphi) + (1 - \cos 2\vartheta)^2 \|h_{x+y}\|^2 + \right. \right. \\ & \left. \left. + 2|(1 - \cos 2\vartheta)(3 + \cos 2\vartheta) \cos 2\varphi| \|h_{x-y}\| \|h_{x+y}\| \right] \cdot \left[ (3 + \cos 2\vartheta)^2 (4\|h_{xy}\|^2 \sin^2 2\varphi + \|h_{x-y}\|^2 \cos^2 2\varphi) + \right. \right. \\ & \left. \left. + (1 - \cos 2\vartheta)^2 THD_{x+y}^2 \|h_{x+y}\|^2 + 2(1 - \cos 2\vartheta)(3 + \cos 2\vartheta) \cos 2\varphi \langle h_{x-y}, h_{x+y} \rangle \right]^{-1} \right\}^{1/2}, \end{aligned} \quad (27)$$

The first of (26) follows immediately from (21); the second one is obtained from (22) using Schwartz inequality. The supremum of the function  $Q(\vartheta, \varphi, e)$  occurs at  $\vartheta = \pi/2$ ,  $\varphi = m\pi$ ,  $\forall e$ , where  $Q(\pi/2, m\pi, e) \lesssim 1.5$  (see *fig. 6*).

The truncation orders required to keep  $THD_{\times,+} \leq 0.01$ , deduced from (26) are collected in *Table-I*.

$e_0$	$N_T$
.1	4
.2	6
.3	8
.4	11
.5	15
.6	22
.7	36
.8	68
.9	206

Table I - Truncation orders needed to keep  $THD_{\times,+} \leq .1$ .

#### 4A A GENERALIZED CARLINI-MEISSEL FORMULA

A key issue for an efficient computation of waveform-templates based on (10), (11) and (12) involves clever evaluation of terms like:

$$J_n(ne), J_{n\pm 1}(ne), J_{n\pm 2}(ne). \quad (28)$$

It is well known that, in general, whenever the argument and the order are close (here, in fact they are proportional through the orbital eccentricity  $e$ ), numerical computation of Bessel functions either by series summation (Abramowitz and Stegun, 1968, ch. X), or by (re-normalized, downward) recurrence (Press et al, 1992, Sect. 6.5) is inefficient. As a convenient alternative, we suggest the following generalization of the well-known (see Watson, 1976, ch. XVII) Carlini-Meissel (henceforth CM) expansion:

$$J_{n\pm k}(ne) \sim J_n^{(CM)}(ne) \Psi_{\pm k}(n, e), \quad (29)$$

where (see Appendix C for the detailed deduction):

$$J_n^{(CM)}(ne) = \frac{\left(\frac{ne}{2}\right)^n}{n!} \left(\frac{1 + \sqrt{1 - e^2}}{2}\right)^{-n} (1 - e^2)^{-1/4} \cdot \exp \left\{ n \left[ \sqrt{1 - e^2} - 1 \right] + n^{-1} \left[ \frac{-3e^2 - 2}{24(1 - e^2)^{3/2}} + \frac{1}{12} \right] \right\}, \quad (30)$$

$$\Psi_{\pm k}(n, e) = \frac{n!}{(n \pm k)!} \left(\frac{ne}{1 + \sqrt{1 - e^2}}\right)^{\pm k} \cdot \exp \left\{ \frac{1}{n} \left[ \mp k \frac{e^2}{1 - e^2} + \frac{k^2}{2} \left(1 - \frac{1}{\sqrt{1 - e^2}}\right) \right] \right\}. \quad (31)$$

Using (31) to evaluate the Fourier coefficients  $\tilde{h}^{(n)}$  does *not* significantly spoil the accuracy of the waveforms. Indeed, spectral truncation according to Table-I still yields THD values below 0.1.

## 5 PROTOTYPE SOURCES

As an application of the above, we wrote a code for waveform template construction, and used it to compute the waveforms for several prototype sources. Taylor et al. (1993) provide data for 24 binary pulsars. In *Table II* we quote *PSR 1913+16* and *PSR 1534+12*, as possible paradigm sources for space detectors, being respectively the most popular and closest known binary pulsars.

Binary	1534+12	1913+16
Right ascension <i>B</i> 1950	15:34:47.686	19:13:12.46769
Declination <i>B</i> 1950	+12:05:45.23	+16:01:08.0323
Orbital inclination <i>i</i> [degrees]	74	45
Distance [kpc]	0.68	7.13
Projected semimajor axis $a_i \sin i$ [light · s]	3.729468	2.3417592
Eccentricity <i>e</i>	0.2736779	0.6171308
Orbital period $P_b$ [d]	0.4207372998	0.322997462736
Companion masses [ $M_\odot$ ]	1.34, 1.34	1.42, 1.41
$\xi_1$ ( $10^{-6}$ )	3.4849	4.3102
$\xi_2$ ( $10^{-3}$ )	1.3200	1.4680
$\xi_3$ ( $10^{-14}$ )	7.6549	13.023
$\Delta$	0	$3.5336 \times 10^{-3}$
$\chi$	434777882.4767	316085232.7313
$h_0$ ( $10^{-23}$ )	16.518	2.0575

*Table II - Paradigm compact binary sources*

The gravitational waveforms at  $\vartheta = \varphi = 0, 45, 90$  deg, computed using 8 harmonics for PSR1534+12 and 22 harmonics for PSR1913+16 (consistent with *Table-I*) are displayed in *fig.s 7.1-7.15*, and *fig.s 8.1-8.15*, respectively. By comparison, the waveforms corresponding to  $e = 0$  are also drawn.

## 6 CONCLUSIONS

The main results in this paper can be summarized as follows. Orbital eccentricity should not be neglected in detecting gravitational waves from steady-state binaries, for which the simple Peters Mathews model has been shown to be accurate enough. GW spectral truncation criteria have been discussed, and computationally efficient tools/techniques have been introduced for constructing reliable templates. We stress that the above tools/techniques could be readily extended, to higher order PN models with relative ease.

## ACKNOWLEDGEMENTS

V. Pierro has been a Visiting Scientist at the European Space Research & Technology Centre ESTEC-ESA, under a grant from the University of Salerno; A.D.A.M. Spallicci, formerly staff at ESTEC-ESA, has been a Visiting Professor at the University of Salerno in 1996. Both wish to express their appreciation to the hosting Institutions.

## REFERENCES

- Abramowitz M., Stegun I.A., 1968, *Handbook of Mathematical Functions*, Dover, New York.  
 Th. Apostolatos, 1996, Phys. Rev. D52, 605, 1996.  
 Barone F. et al., 1988, Astron. Astrophys., 199, 161.  
 Bertotti B. et al., 1999, Phys. Rev. D59, 082001, 1999.  
 Eggleton P.P., 1983, Ap. J. 268, 368.  
 Hils D. et al., 1992, Ap. J. 360, 75.  
 K. Martel and E. Poisson, Phys. Rev. D60, 124008, 1999.  
 Moreno-Garrido C. et al., 1994, MNRAS, 266, 16.  
 Moreno-Garrido C. et al., 1995, MNRAS, 274, 115.  
 Peters P.C., 1964, Phys. Rev., 136, 4B, 1124.  
 Peters P.C., Mathews J., 1963, Phys. Rev., 131, 435.  
 Pierro V., Pinto I., 1996a, Nuovo Cimento B 111, 631.  
 Pierro V., Pinto I., 1996b, Nuovo Cimento B 111, 1517.  
 Pierro V., Pinto I., 1996c, Ap. J., 469, 272.  
 Poisson E. , 1993, Phys. Rev D, 47, 1497.  
 Press W.H. et al., 1992, *Numerical Recipes*, Cambridge Univ. Press.  
 Taylor J.H. et al., 1993, Ap. J. Suppl. Ser., 88, 529.  
 Wahlquist H., 1987, Gen. Rel. Grav., 19, 1101.  
 Watson G.N., 1966, *A Treatise on the Theory of Bessel Functions*, Cambridge Un. Press.  
 Schott G.A., *Electromagnetic Radiation*, Cambridge, 1912.  
 Prudnikov A.P. et al., *Integrals and Series*, Gordon and Breach, 1986.

## APPENDIX A: RELEVANT TO EQ.S (10) TO (16).

In the weak-field slow-motion approximation, the cartesian far-field harmonic-gauge metric tensor deviation components in (8), (9) are simply related to the source quadrupole tensor  $I_{ij}$  through:

$$h_{xy} = \frac{2G}{c^4 r} \frac{d^2 I_{xy}}{dt^2}, \quad h_{xx} = \frac{2G}{c^4 r} \frac{d^2 I_{xx}}{dt^2}, \quad h_{yy} = \frac{2G}{c^4 r} \frac{d^2 I_{yy}}{dt^2}, \quad (A1)$$

where:

$$I_{xx} = \mu \rho^2 \cos^2(\phi), \quad I_{yy} = \mu \rho^2 \sin^2(\phi), \quad I_{xy} = \mu \rho^2 \cos(\phi) \sin(\phi), \quad (A2)$$

$\rho$  being the companion star separation,  $e$  the eccentricity,  $\phi$  the true anomaly and  $\mu$  the reduced mass.

The relevant terms of the (reduced) quadrupole moment can be conveniently rewritten:

$$I_{xx} = \mu a^2 \xi^2, \quad I_{yy} = \mu a^2 \eta^2, \quad I_{xy} = \mu a^2 \xi \eta, \quad (A3)$$

where  $a$  is the orbit semimajor axis,

$$\xi = \left( \frac{\rho \cos \phi}{a} \right), \quad \eta = \left( \frac{\rho \sin \phi}{a} \right). \quad (A4)$$

Then, using the well known Keplerian equations (see, e.g., Watson, 1976, ch. XVII)

$$\frac{\rho \cos \phi}{a} = \cos E - e, \quad \frac{\rho \sin \phi}{a} = (1 - e^2)^{1/2} \sin E, \quad (A5)$$

where  $E$  is the eccentric anomaly, and the relation between the latter and the mean anomaly  $M$ ,

$$M = \frac{2\pi t}{T} = E - e \sin E, \quad (A6)$$

one can expand  $\xi^2$ ,  $\eta^2$  and  $\xi\eta$  into Fourier series of argument  $M$ , taking properly into account their parities, viz.:

$$\xi^2 = \frac{\gamma_0}{2} + \sum_{n=1}^{\infty} \gamma_n \cos(nM), \quad (A7)$$

$$\eta^2 = \frac{\delta_0}{2} + \sum_{n=1}^{\infty} \delta_n \cos(nM), \quad (A8)$$

$$\xi\eta = \sum_{n=1}^{\infty} \eta_n \sin(nM). \quad (A9)$$

The relevant Fourier coefficients are readily found. Hence, using (A5) and (A6):

$$\gamma_n = \frac{2}{n\pi} \int_0^{\pi} \sin[n(E - e \sin E)] (\sin 2E - 2e \sin E) dE, \quad (A10)$$

$$\delta_n = -\frac{2}{n\pi} (1 - e^2) \int_0^{\pi} \sin[n(E - e \sin E)] \sin 2E dE, \quad (A11)$$

$$\eta_n = \frac{2}{n\pi} (1 - e^2)^{1/2} \int_0^{\pi} \cos[n(E - e \sin E)] (\cos 2E - e \cos E) dE. \quad (A12)$$

Upon repeated use of trivial trigonometric identities, and in view of the integral definition of the Bessel function of the 1st kind,

$$J_{\nu}(\alpha) = \frac{1}{\pi} \int_0^{\pi} \cos[\nu x - \alpha \sin x] dx, \quad (A13)$$

the Fourier coefficients (A10) to (A12) can be written:

$$\gamma_n = \frac{1}{n} [J_{n-2}(ne) - J_{n+2}(ne)] - \frac{2e}{n} [J_{n-1}(ne) - J_{n+1}(ne)], \quad (A14)$$

$$\delta_n = -\frac{1}{n} (1 - e^2) [J_{n-2}(ne) - J_{n+2}(ne)], \quad (A15)$$

$$\eta_n = \frac{1}{n} (1 - e^2)^{1/2} [J_{n-2}(ne) + J_{n+2}(ne) - 2J_n(ne)]. \quad (A16)$$

Using (A14) to (A16) and (A7) to (A9) in (A1) to (A3) gives equations (10) to (16).

## APPENDIX B: RELEVANT TO EQUATIONS (22) – (26)

In order to establish eq.s (22) to (26) one may repeatedly use the recurrency formula:

$$J_{n\pm 1}(z) = \frac{n}{z} J_n(z) \pm J'_n(z), \quad (B1)$$

so as to reduce the sought series to combinations of the following (generalized) Kapteyn's expansions of the second kind:

$$\sum_{n=1}^{\infty} n^2 [J'_n(ne)]^2, \quad (B2)$$

$$\sum_{n=1}^{\infty} [J'_n(ne)]^2, \quad (B3)$$

$$\sum_{n=1}^{\infty} \frac{[J'_n(ne)]^2}{n^2}, \quad (B4)$$

$$\sum_{n=1}^{\infty} n^2 J_n^2(ne), \quad (B5)$$

$$\sum_{n=1}^{\infty} J_n^2(ne), \quad (B6)$$

$$\sum_{n=1}^{\infty} n J_n(ne) J'_n(ne). \quad (B7)$$

These latter can be summed as follows. From the Fourier analysis of Kepler motion, the following equations are readily established (see, e.g., Watson, 1966), ch. 17.2 :



$$\cos E = -\frac{e}{2} + 2 \sum_{n=1}^{\infty} \frac{J'_n(ne)}{n} \cos nM, \quad (B8)$$

$$\sin E = \frac{2}{e} \sum_{n=1}^{\infty} \frac{J_n(ne)}{n} \sin nM, \quad (B9)$$

$$\frac{dE}{dM} = (1 - e \cos E)^{-1}. \quad (B10)$$

Differentiating eq. (B8) w.r.t.  $M$ , and using (B10), one gets:

$$\frac{\sin E}{1 - e \cos E} = 2 \sum_{n=1}^{\infty} J'_n(ne) \sin nM, \quad (B11)$$

$$\frac{\cos E - e}{(1 - e \cos E)^3} = 2 \sum_{n=1}^{\infty} n J'_n(ne) \cos nM. \quad (B12)$$

Similarly, from (B9):

$$\frac{\cos E}{1 - e \cos E} = \frac{2}{e} \sum_{n=1}^{\infty} J_n(ne) \cos(nM), \quad (B13)$$

$$\frac{\sin E}{(1 - e \cos E)^3} = \frac{2}{e} \sum_{n=1}^{\infty} n J_n(ne) \sin(nM), \quad (B14)$$

where  $E$  is the eccentric anomaly,  $M$  the mean anomaly, and  $e$  the eccentricity. The following procedure can be then applied to eq.s (B8) and (B11)-(B14): *i*) squaring; *ii*) taking the average in  $M$  over  $(0, 2\pi)$ , using again eq. (B10); *iii*) using the well known (Euler) transformations:

$$\cos E = (z + z^{-1})/2, \quad \sin E = -i(z - z^{-1})/2, \quad dE = -iz^{-1} dz,$$

so as to express the sought series as contour integrals on  $|z|=1$  of rational functions of  $z$ , which are trivially computed in terms of residues.

As an example, applying the above procedure to eq. (B13), one gets:

$$\begin{aligned} \frac{4}{e^2} \sum_{n=1}^{\infty} J_n^2(ne) &= \frac{1}{2\pi} \int_0^{2\pi} \frac{\cos^2 E}{1 - e \cos E} dE = \frac{1}{2\pi i} \oint_{|z|=1} \frac{(1+z^2)^2}{z^2[4z - 2e(1+z^2)]} dz = \\ &= \sum_{|z_i| < 1} \text{Res} \left[ \frac{(1+z^2)^2}{z^2[4z - 2e(1+z^2)]} \right]_{z=z_i}. \end{aligned} \quad (B15)$$

The integrand function on the r.h.s. of (B15) has a double pole at  $z=0$  and two simple ones at  $z = (2e)^{-1}[1 \mp (1 - e^2)^{1/2}]$ . Only two poles above fall within  $|z| < 1$ , and (B15) gives:

$$\sum_{n=1}^{\infty} J_n^2(ne) = \frac{1}{2} [(1 - e^2)^{-1/2} - 1] \quad (B16)$$

in agreement with Watson, ch. 17.6, eq. (2). Similarly, starting from (B8), (B11), (B13) and (B14) one gets, respectively  $\dagger\dagger$ :

$$\sum_{n=1}^{\infty} \frac{[J'_n(ne)]^2}{n^2} = \frac{1}{2} \left( 1 - \frac{e^2}{4} \right), \quad (B17)$$

$$\sum_{n=1}^{\infty} [J'_n(ne)]^2 = \frac{1}{2e^2} [1 - (1 - e^2)^{1/2}], \quad (B18)$$

$$\sum_{n=1}^{\infty} n^2 [J'_n(ne)]^2 = \frac{4 + 3e^2}{8(1 - e^2)^{5/2}}, \quad (B19)$$

$\dagger\dagger$  Note that equation (3) in Watson ch. 17.6, is in error, as seen by comparison with (B20), and by direct numerical check. For this (erroneous) result Watson quotes (Schott, 1912). The same error appears in (Prudnikov et al., 1986, sect. 5.7.31).

$$\sum_{n=1}^{\infty} n^2 J_n^2(ne) = \frac{e^2(4+e^2)}{16(1-e^2)^{7/2}}. \quad (B20)$$

The series (B7) can be summed by differentiating both sides of eq. (B16) w.r.t.  $e$ . Hence:

$$\sum_{n=1}^{\infty} n J_n(ne) J_n'(ne) = \frac{e}{4(1-e^2)^{3/2}}. \quad (B21)$$

### APPENDIX C: GENERALIZED CARLINI-MEISSEL EXPANSIONS

To obtain the generalized Carlini Meissel expansion for  $J_{n\pm k}(ne)$  we start from Bessel equation for  $J_{n\pm k}(ne)$ :

$$\frac{d^2 J_{n\pm k}(ne)}{de^2} + \frac{1}{e} \frac{dJ_{n\pm k}(ne)}{de} + \left[ n^2 - \frac{(n\pm k)^2}{e^2} \right] J_{n\pm k}(ne) = 0, \quad (C1)$$

and let<sup>††</sup>:

$$J_n(ne) = J_{n\pm k}(ne) = \frac{n^{(n\pm k)}}{(n\pm k)!} \exp \left[ \int_0^e u_{n\pm k}(z) dz \right]. \quad (C2)$$

On letting eq.s (C2) into (C1), we get:

$$\dot{u}_{n\pm k} + u_{n\pm k}^2 + e^{-1} u_{n\pm k} + n^2 - \frac{(n\pm k)^2}{e^2} = 0, \quad (C3)$$

then, following Carlini and Meissel, we assume that the following *asymptotic* representation for  $u_{n\pm k}$ , ( $k = 0, 1, 2$ ) holds:

$$u_{n\pm k}(z) \approx \frac{u_{n\pm k}^-(z)}{n} + u_{n\pm k}^0(z) + n u_{n\pm k}^+(z). \quad (C4)$$

Substituting (C4) into (C3), and equating like powers of  $n$  (as required by consistency), we get:

$$u_{n\pm k}^+ = \frac{\sqrt{1-z^2}}{z}, \quad (C5)$$

$$u_{n\pm k}^0 = \frac{\pm 2k - e u_{n\pm k}^+ - e^2 \dot{u}_{n\pm k}^+}{2e^2 u_{n\pm k}^+}, \quad (C6)$$

$$u_{n\pm k}^- = \frac{k^2 - e u_{n\pm k}^0 - e^2 [\dot{u}_{n\pm k}^0 + (u_{n\pm k}^0)^2]}{2e^2 u_{n\pm k}^+}. \quad (C7)$$

Hence:

$$u_{n\pm k}^0 = \frac{z}{2(1-z^2)} \pm k \frac{1}{z \sqrt{1-z^2}}, \quad (C8)$$

$$u_{n\pm k}^- = \frac{-z^3 - 4z}{8(1-z^2)^{5/2}} \mp k \frac{z}{(1-z^2)^2} + k^2 \frac{z^3 - z}{2(1-z^2)^{5/2}}. \quad (C9)$$

Carrying out the integrations in (C2), and taking into account that  $J_{n\pm k}(0) = \delta_{n\pm k,0}$  we get:

$$\int_0^e u_{n\pm k}^+(z) dz = \sqrt{1-e^2} + \log \left[ \frac{e}{1+\sqrt{1-e^2}} \right] + C_{n\pm k}^+, \quad (C10)$$

$$\int_0^e u_{n\pm k}^0(z) dz = -\frac{1}{4} \log(1-e^2) \pm k \log \left[ \frac{e}{1+\sqrt{1-e^2}} \right] + C_{n\pm k}^0, \quad (C11)$$

<sup>††</sup> This formula is suggested by the well-known McLaurin expansions of Bessel functions.

$$\int^e u_{n\pm k}^-(z) dz = \frac{-3e^2 - 2}{24(1 - e^2)^{3/2}} \mp k \frac{1}{2(1 - e^2)} + k^2 \frac{e^2 - 1}{2(1 - e^2)^{3/2}} + C_{n\pm k}^- \quad (C12)$$

Plugging the last three eq.s into eq. (C2) we obtain:

$$J_{n\pm k}(ne) = \frac{(ne)^{n\pm k}}{(n \pm k)!} (1 + \sqrt{1 - e^2})^{-(n\pm k)} (1 - e^2)^{-1/4} \cdot \exp \left\{ n \sqrt{1 - e^2} + n^{-1} \left[ \frac{-3e^2 - 2}{24(1 - e^2)^{3/2}} + \mp k \frac{1}{2(1 - e^2)} - k^2 \frac{1 - e^2}{2(1 - e^2)^{3/2}} \right] + n C_{n\pm k}^+ + C_{n\pm k}^0 + n^{-1} C_{n\pm k}^- \right\}. \quad (C13)$$

The unknown integration constants can be found by enforcing the following obvious asymptotic equality, valid for all  $n$ :

$$J_{n\pm k}(e \rightarrow 0) \sim \frac{(ne/2)^{(n\pm k)}}{(n \pm k)!}. \quad (C14)$$

Hence:

$$\begin{cases} 1 + C_{n\pm k}^+ = 0, \\ C_{n\pm k}^0 = 0, \\ -1/12 \mp k/2 - k^2/2 + C_{n\pm k}^- = 0. \end{cases} \quad (C15)$$

Hence, from (C13):

$$J_{n\pm k}(ne) \approx \frac{\left(\frac{ne}{2}\right)^{n\pm k}}{(n \pm k)!} \left(\frac{1 + \sqrt{1 - e^2}}{2}\right)^{-(n\pm k)} (1 - e^2)^{-1/4} \cdot \exp \left\{ n \left[ \sqrt{1 - e^2} - 1 \right] + n^{-1} \left[ \frac{-3e^2 - 2}{24(1 - e^2)^{3/2}} + \mp k \frac{1}{2(1 - e^2)} - k^2 \frac{1 - e^2}{2(1 - e^2)^{3/2}} + \frac{1}{12} \pm \frac{k}{2} + \frac{k^2}{2} \right] \right\}. \quad (C16)$$

The r.h.s. of eq. (C16) above will be henceforth denoted as  $J_{n\pm k}^{CM}(ne)$ , and can be more conveniently written as in (29) to (31).

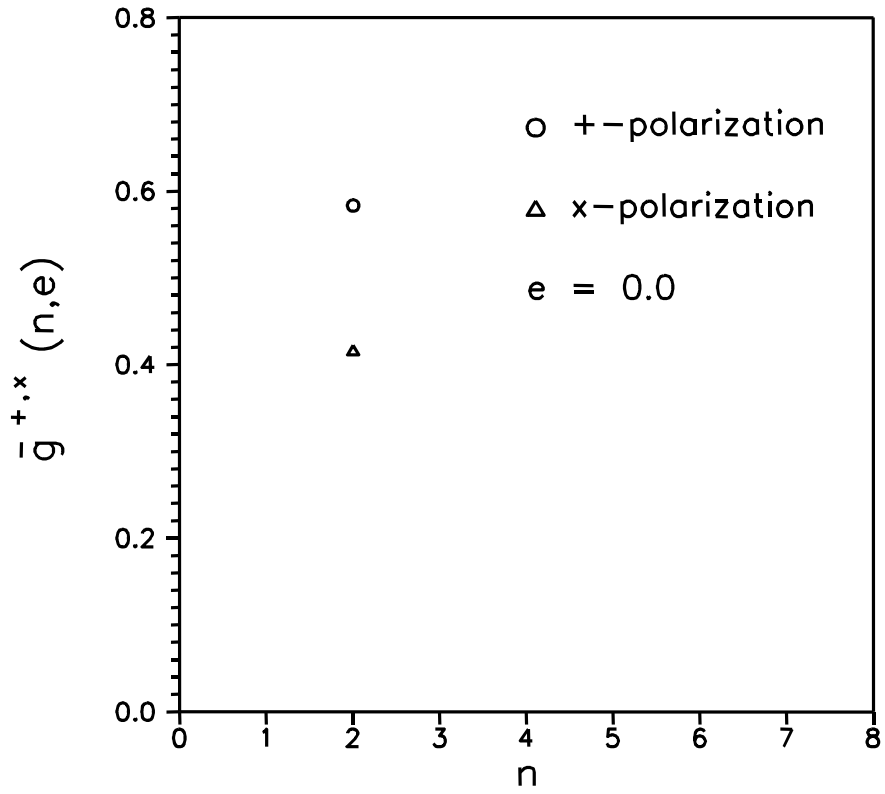
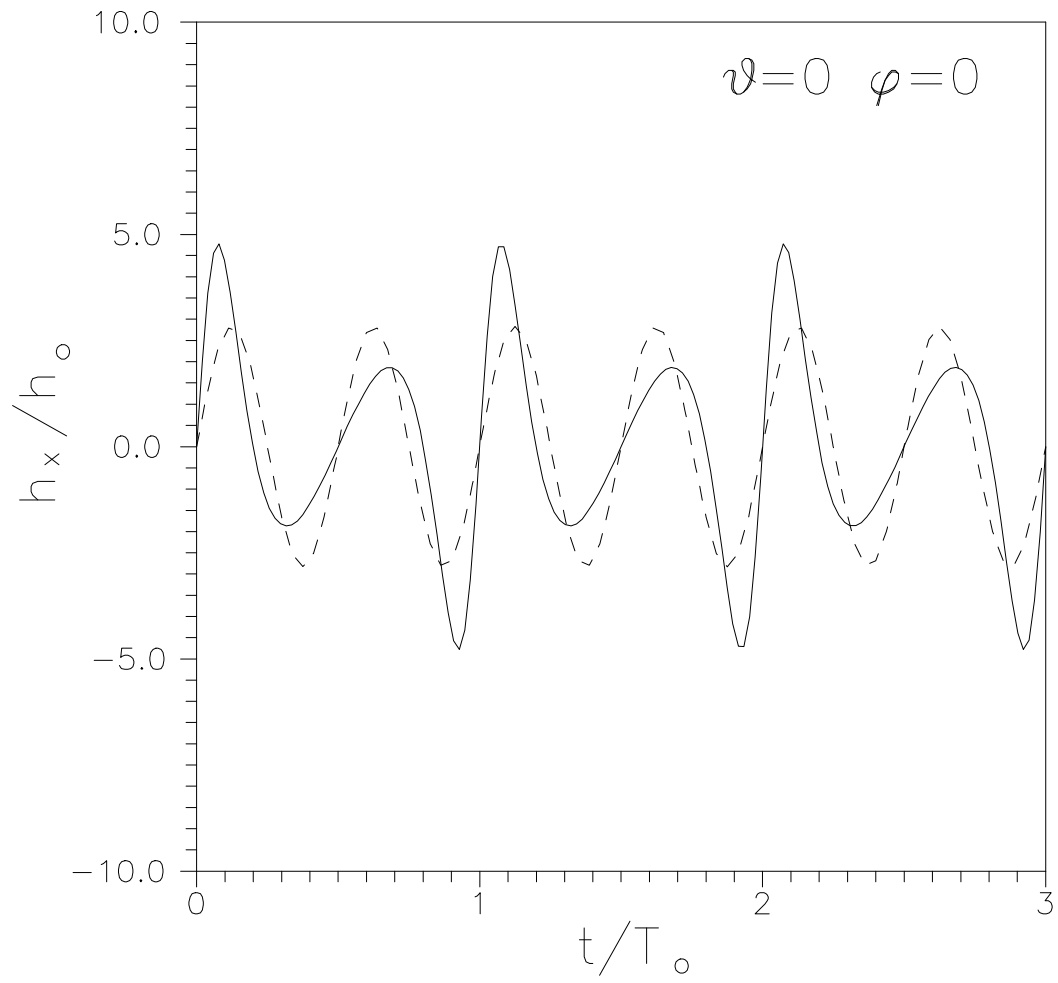
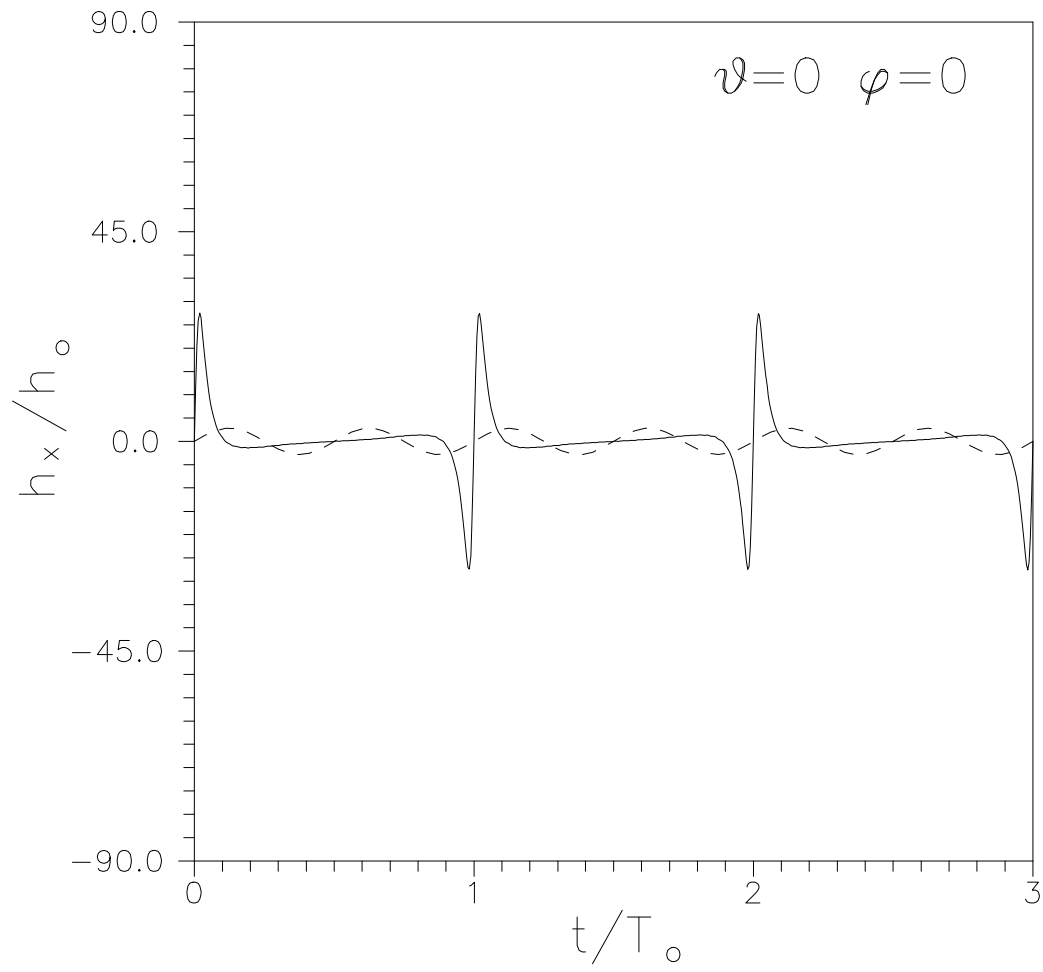


Fig. 1.1 -  $g_{+,x}^{+} (n,0)$ , relevant to eq. (5).



*Fig. 7.1* - PSR1534+12 - a waveform gallery.



*Fig. 8.1* - PSR1913+16 - a waveform gallery.

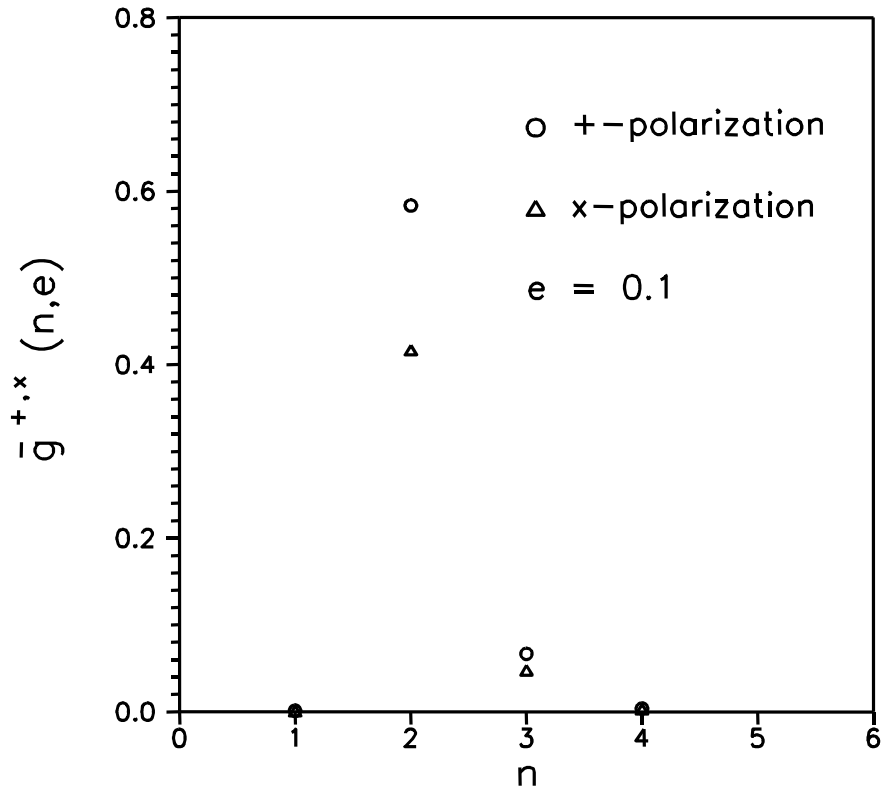
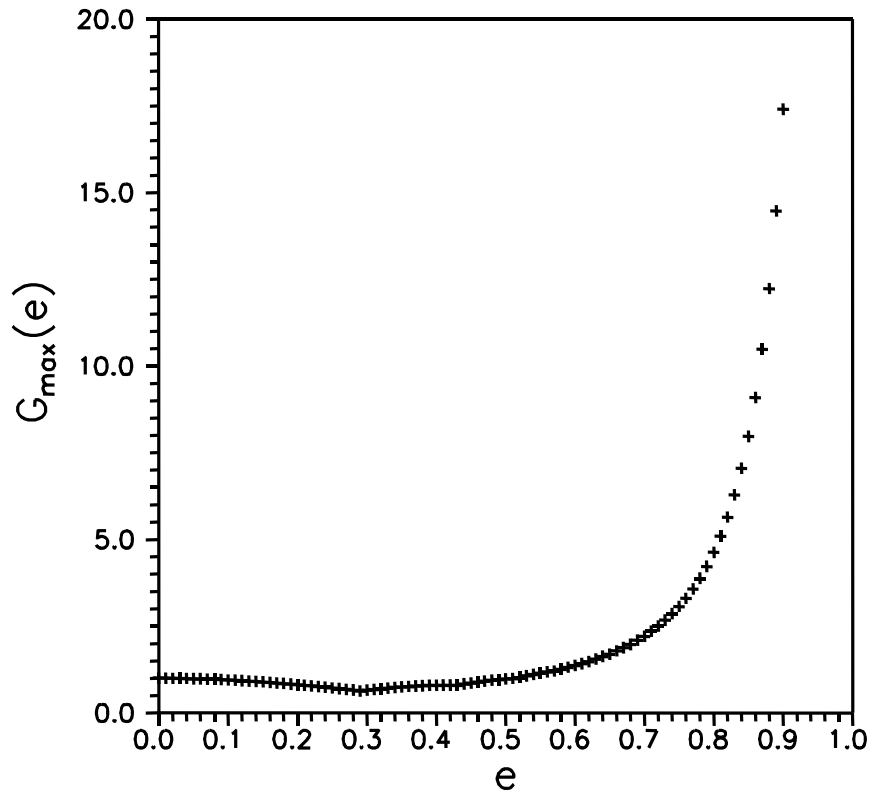
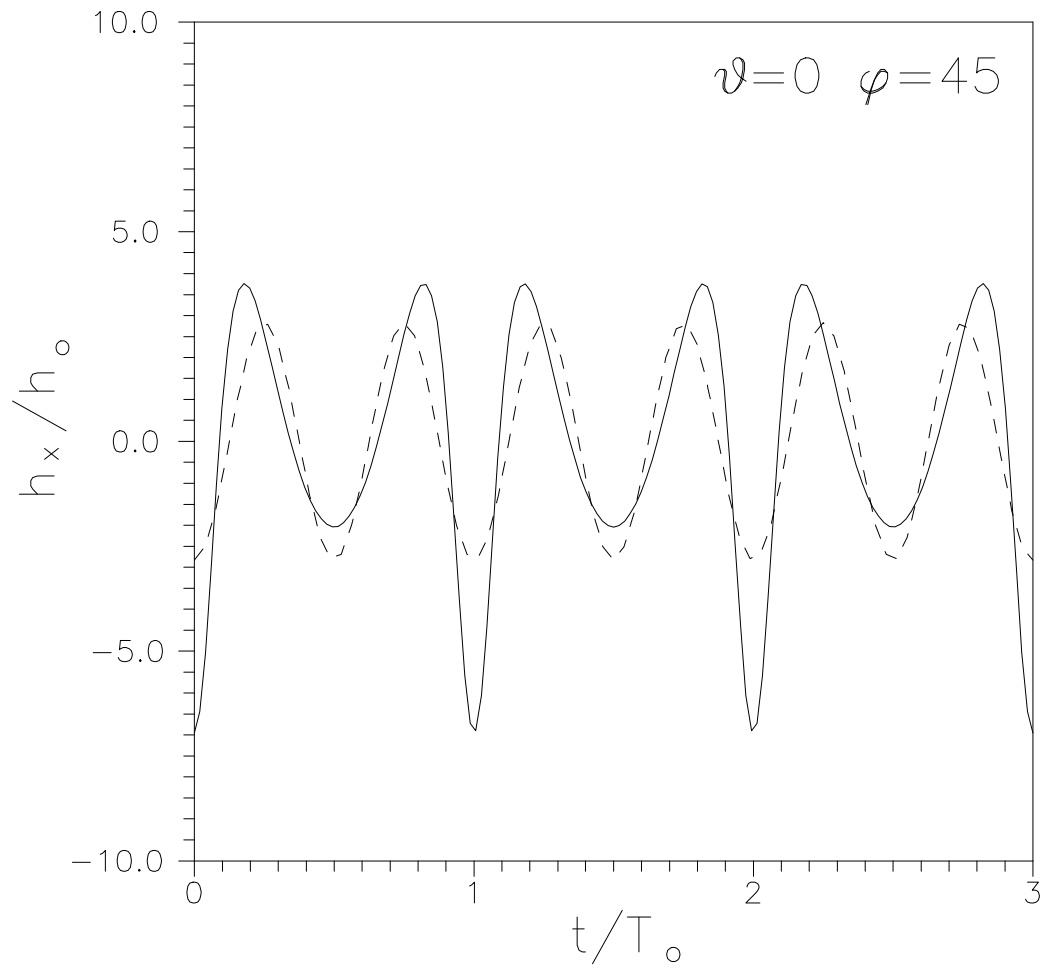


Fig. 1.2 -  $\bar{g}_{+,x}^{+}(n,1)$ , relevant to eq. (5).



*Fig. 2* -  $G_{\max}(e)$ , relevant to eq. (5).





*Fig. 7.2* - PSR1534+12 - a waveform gallery.

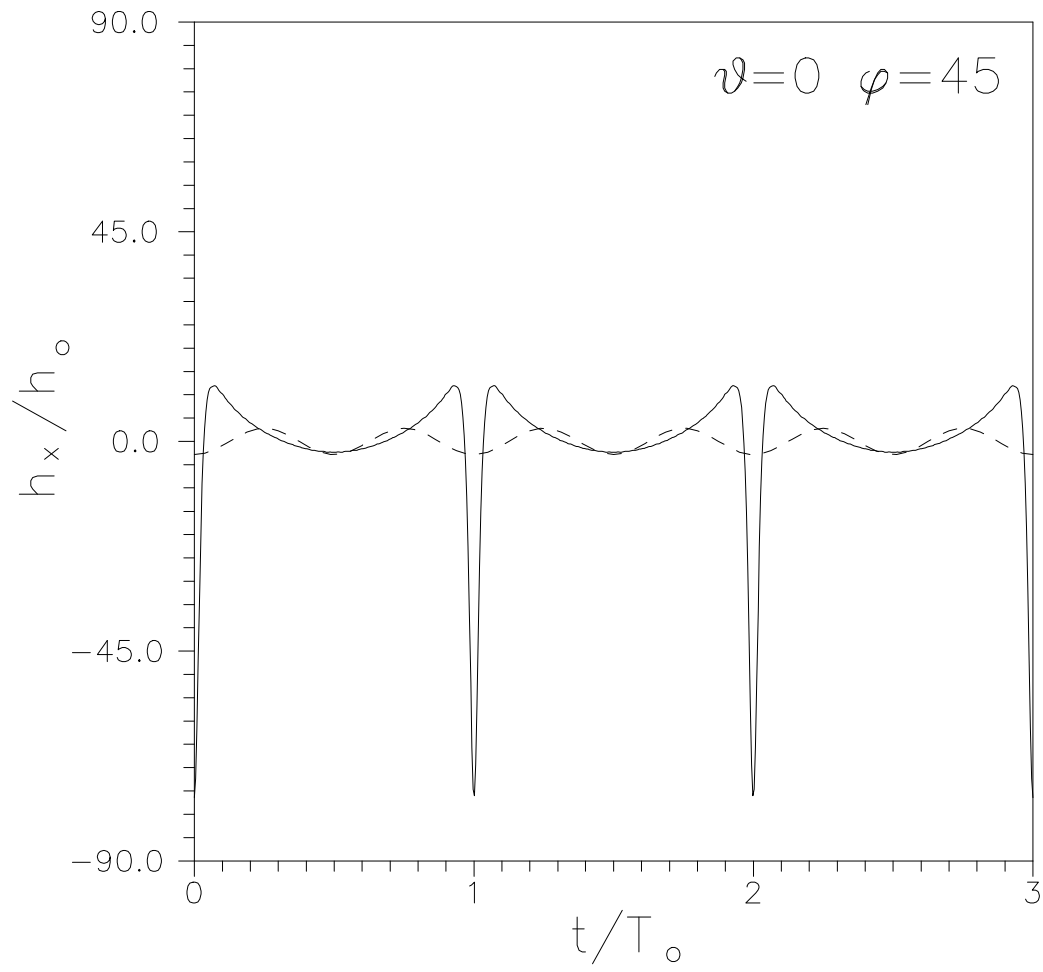


*Fig. 8.2 - PSR1913+16 - a waveform gallery.*

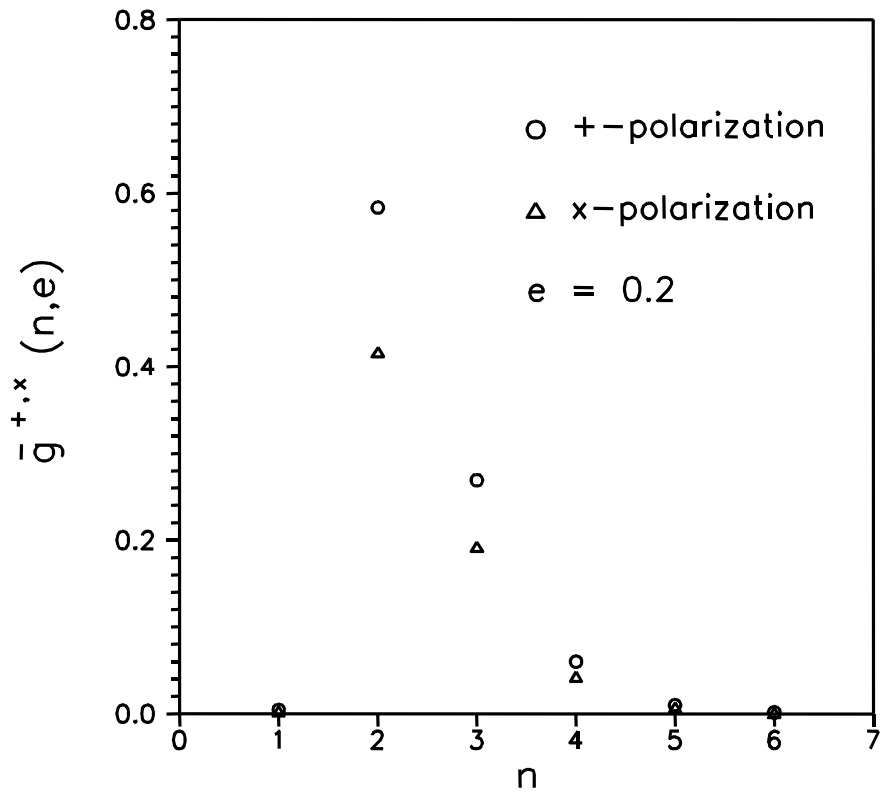
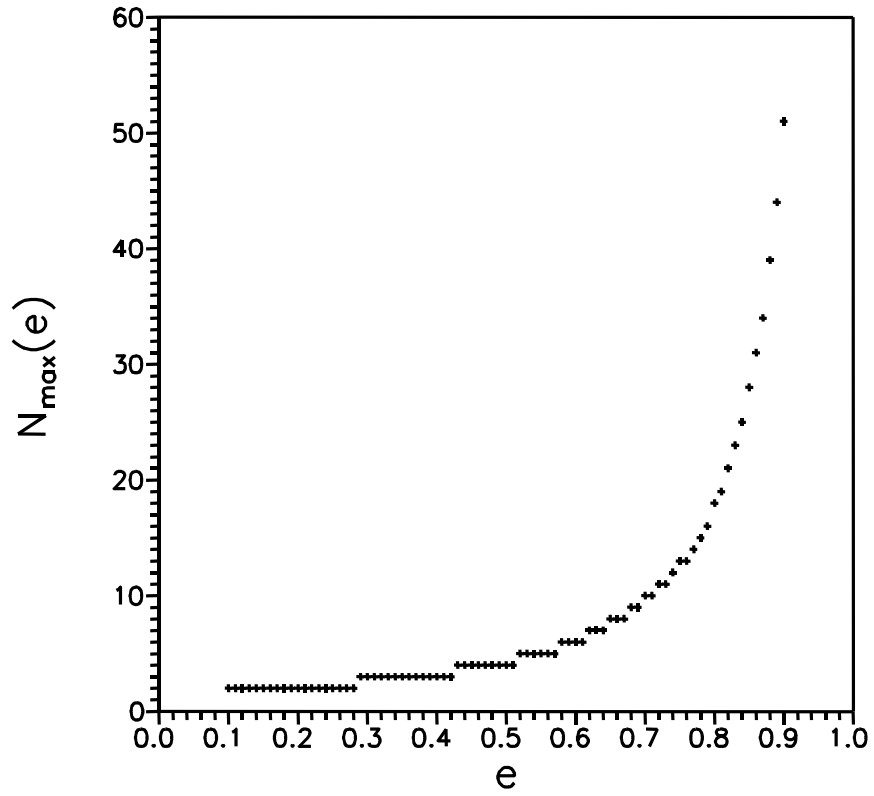
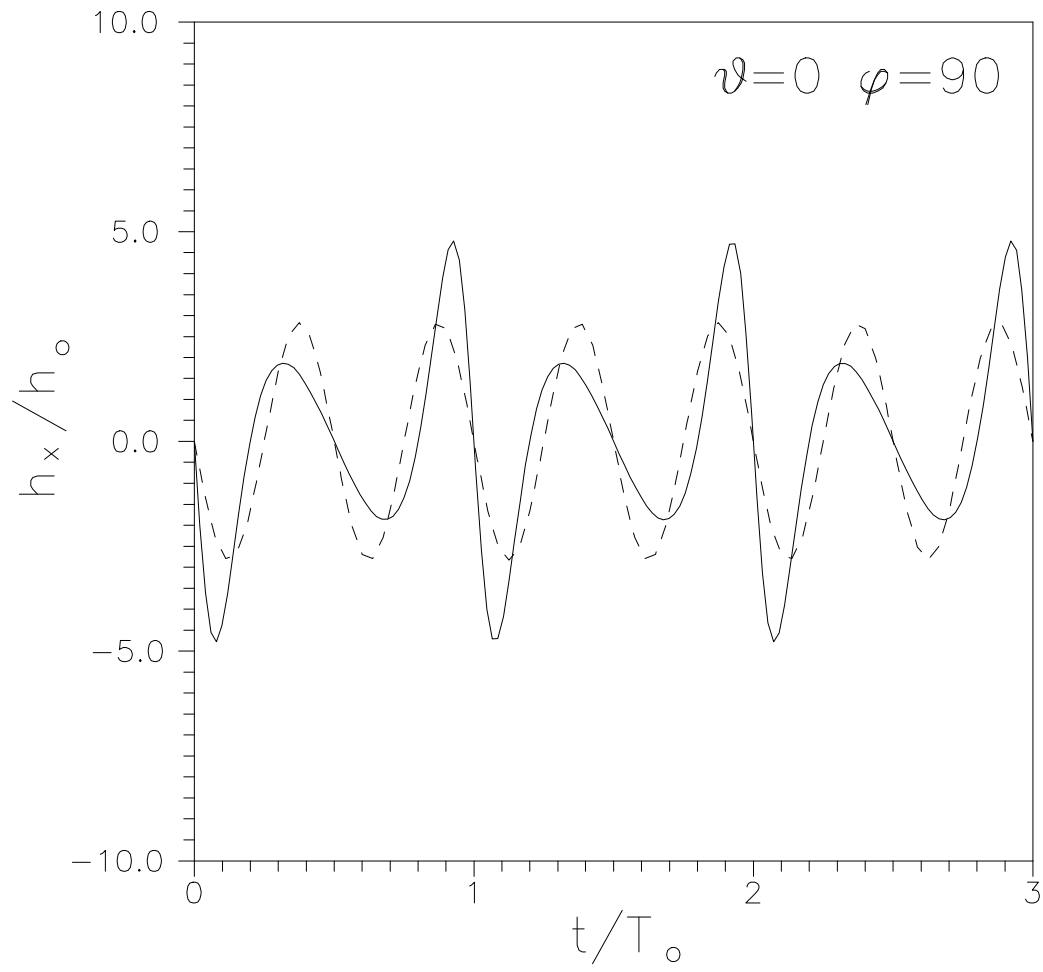


Fig. 1.3 -  $\bar{g}_{+,x}^{+} (n,2)$ , relevant to eq. (5).



*Fig. 3* - $N_{\max}(e)$ , relevant to eq. (5).



*Fig. 7.3 - PSR1534+12 - a waveform gallery.*

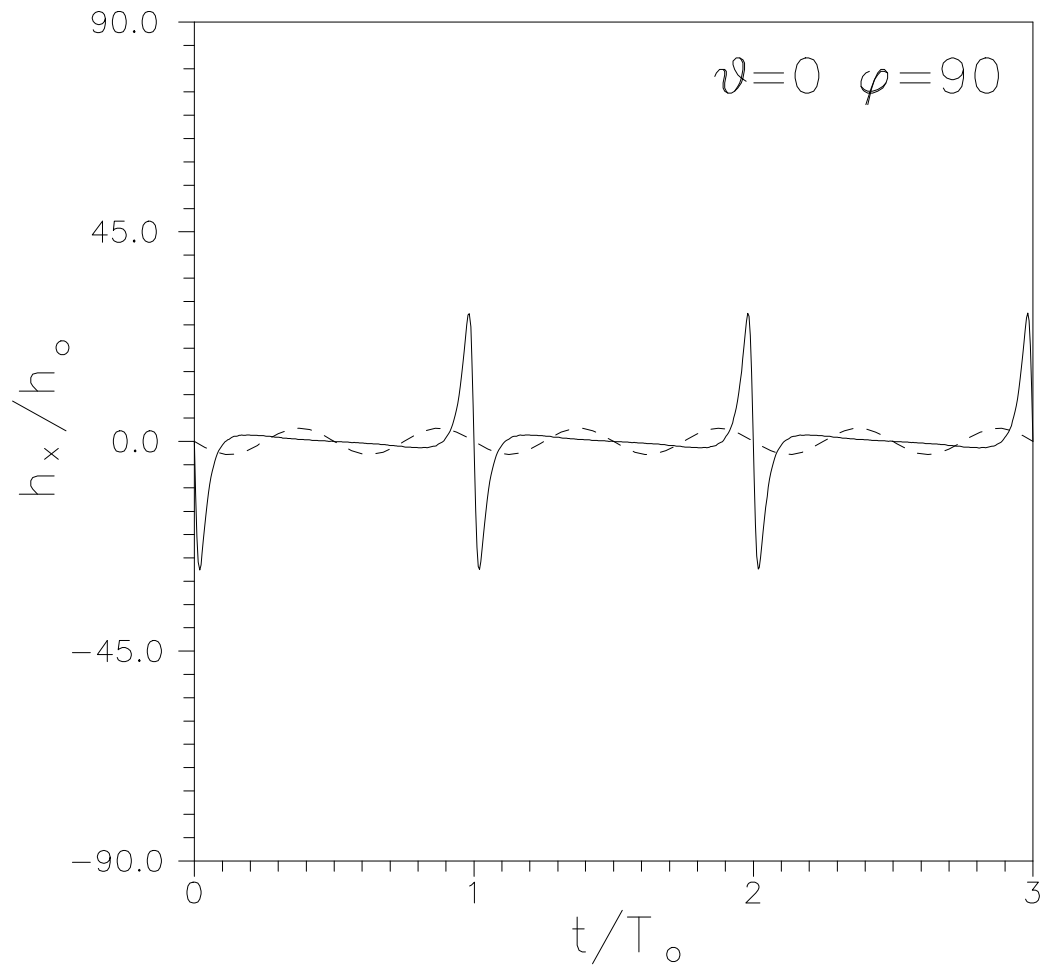


*Fig. 8.3 - PSR1913+16 - a waveform gallery.*

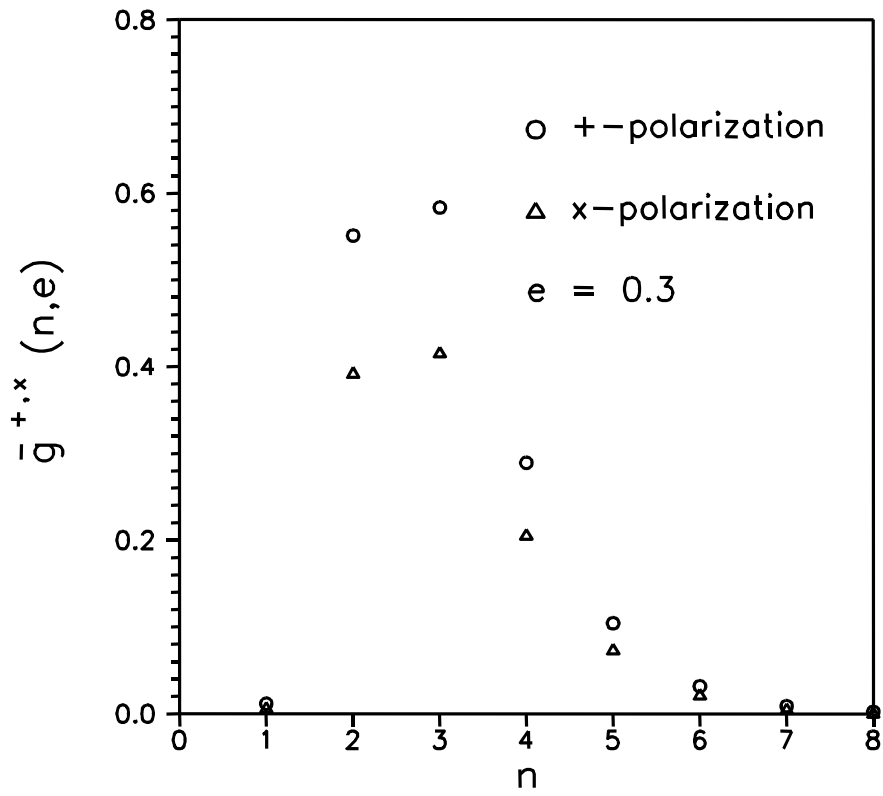
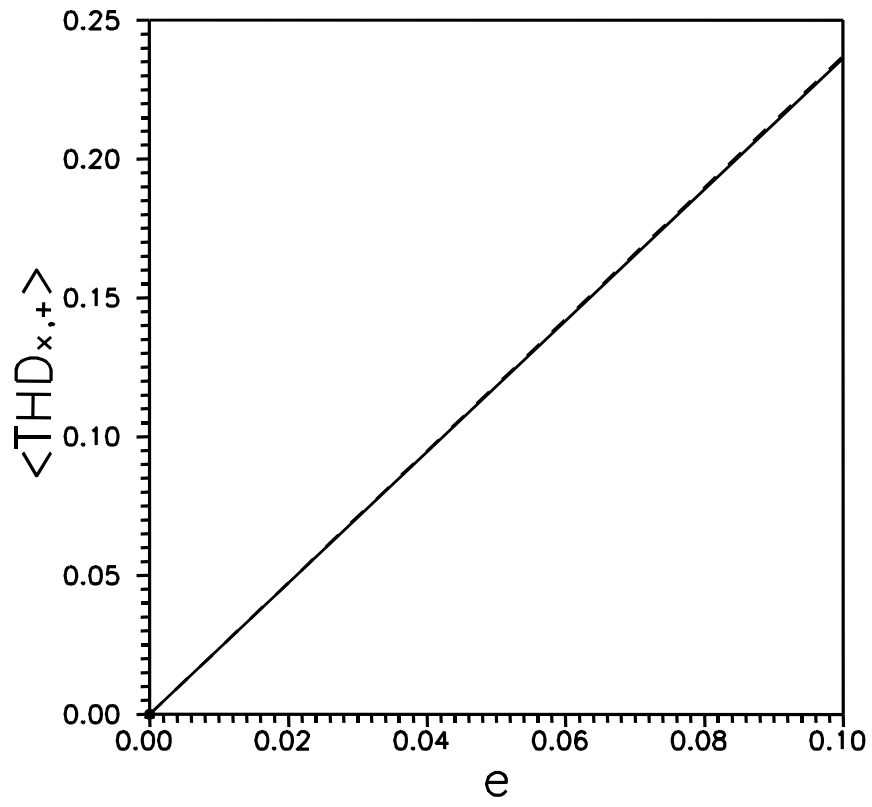
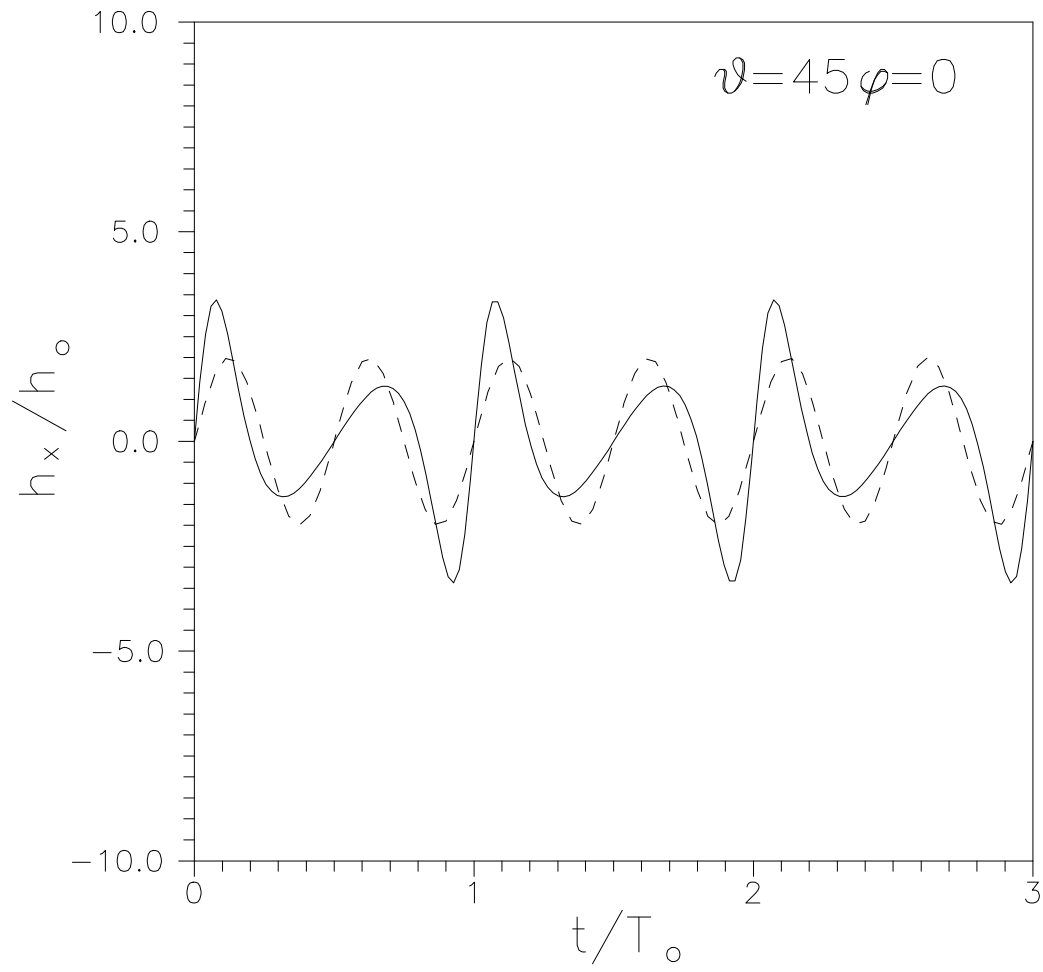


Fig. 1.4 -  $g_{+,x}^{+} (n,3)$ , relevant to eq. (5).



*Fig. 4 - Angle-averaged THD<sub>+,x</sub>.*





*Fig. 7.4* - PSR1534+12 - a waveform gallery.

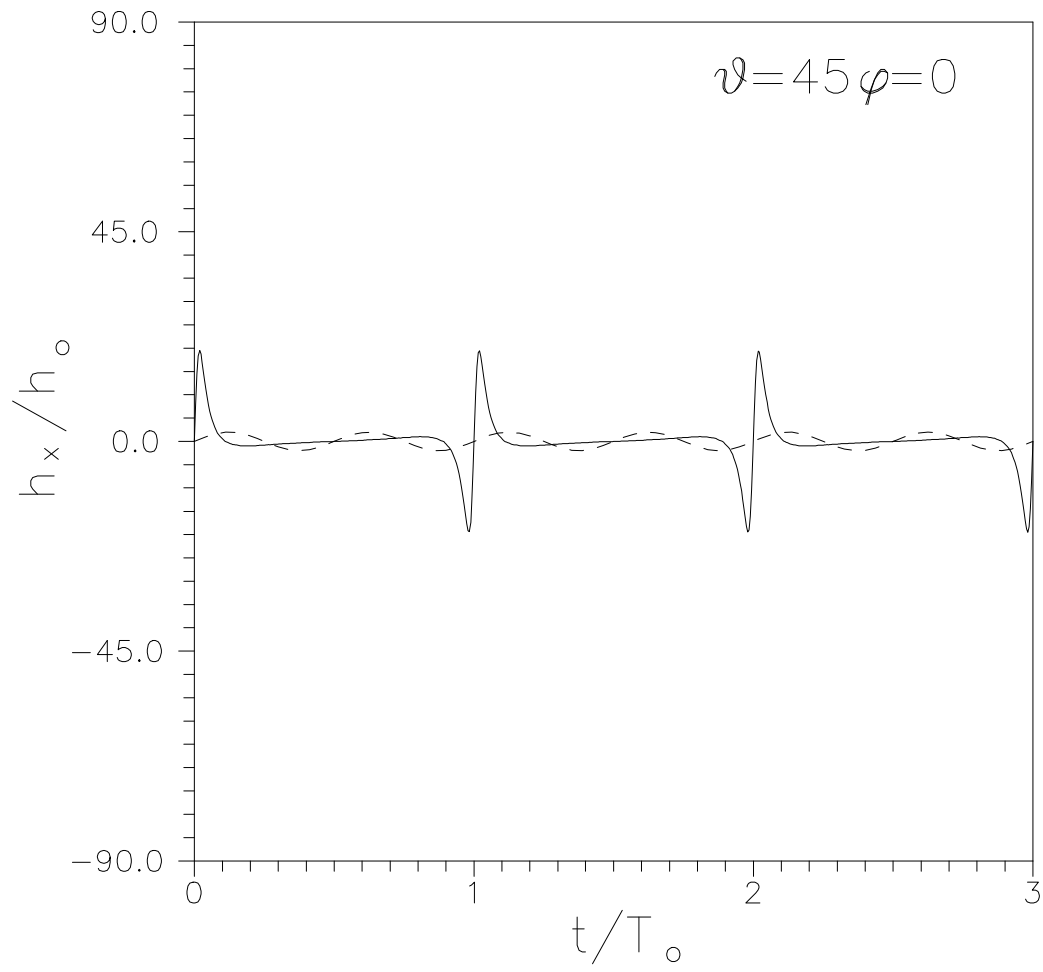


*Fig. 8.4* - PSR1913+16 - a waveform gallery.

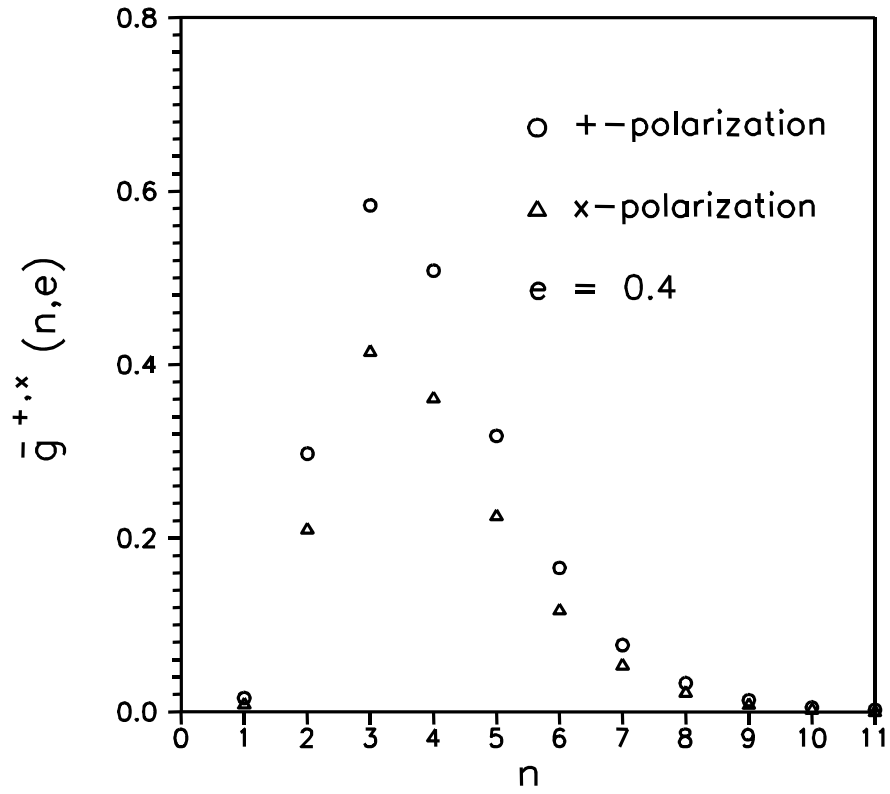


Fig. 1.5 -  $\bar{g}_{+,x}^{+} (n,4)$ , relevant to eq. (5).

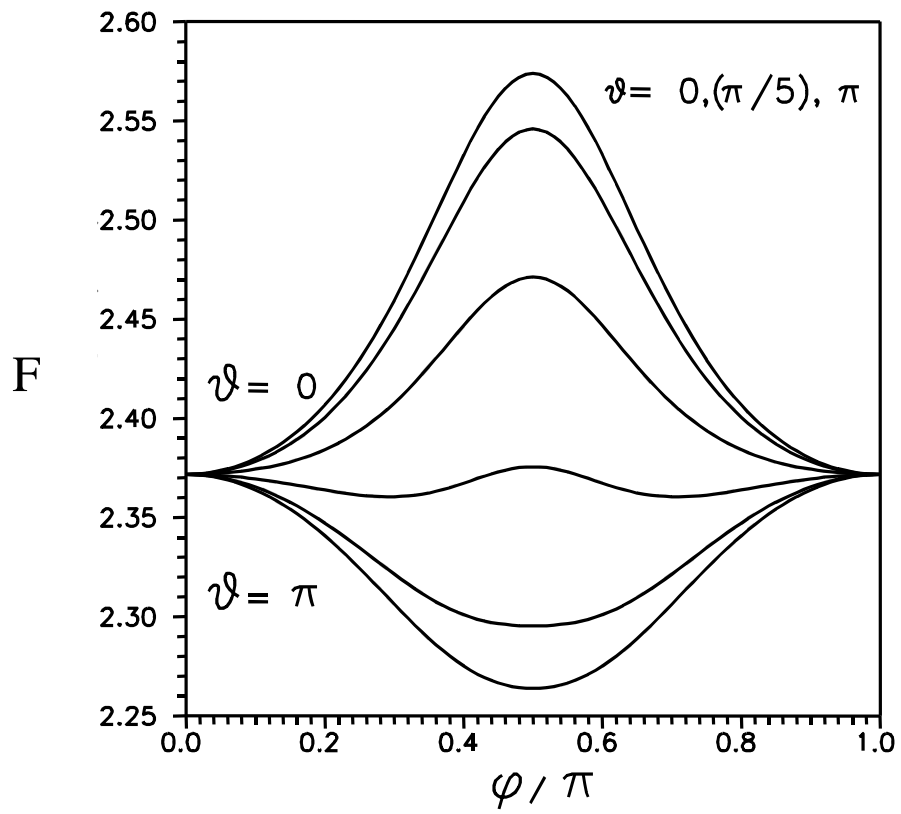
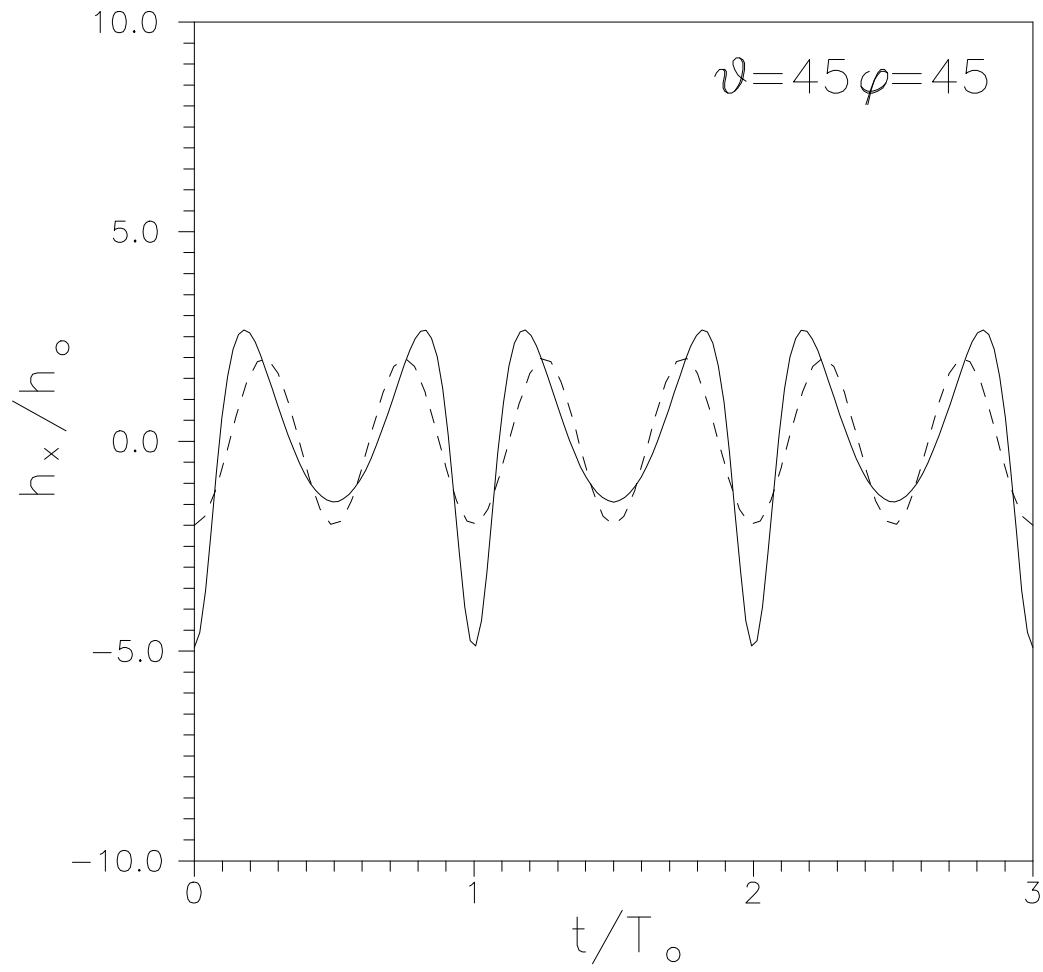
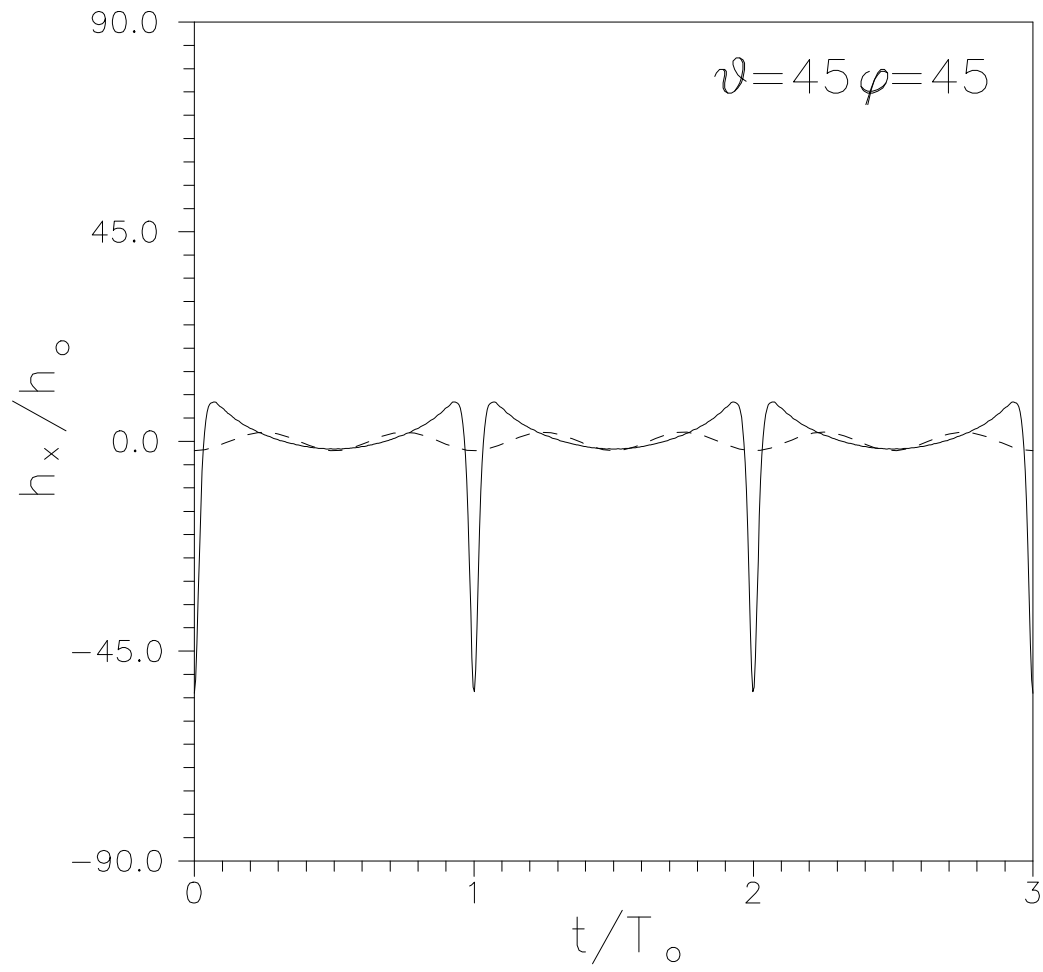


Fig 5 - The angle-dependent factor  $F$  in eq. (25).



*Fig. 7.5 - PSR1534+12 - a waveform gallery.*



*Fig. 8.5* - PSR1913+16 - a waveform gallery.

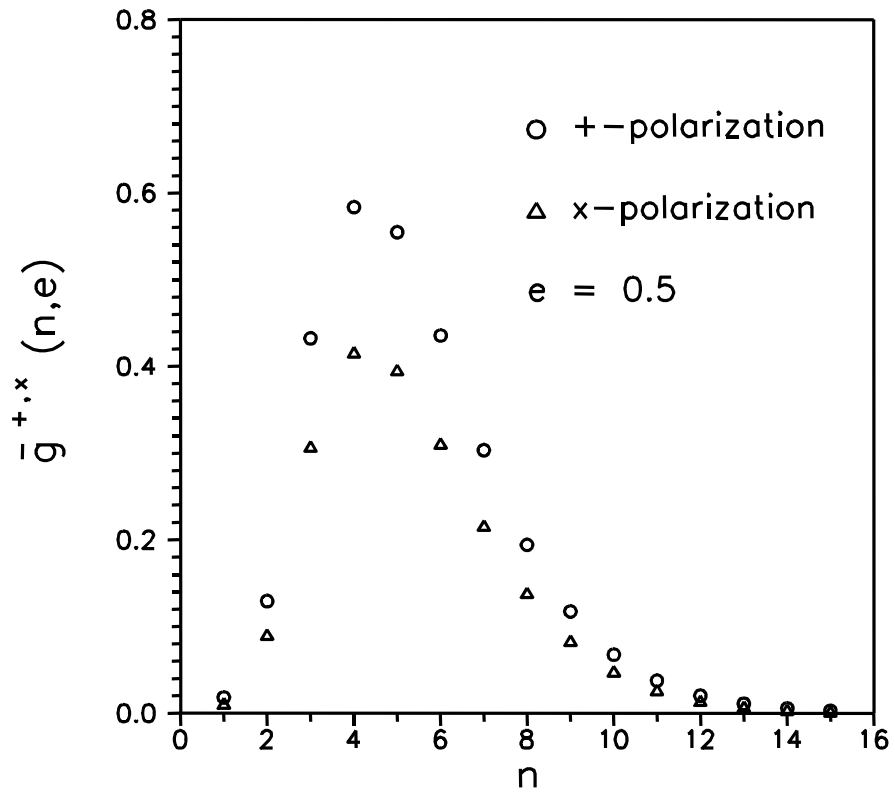


Fig. 1.6 -  $g_{+,x}^{+,x}(n,5)$ , relevant to eq. (5).

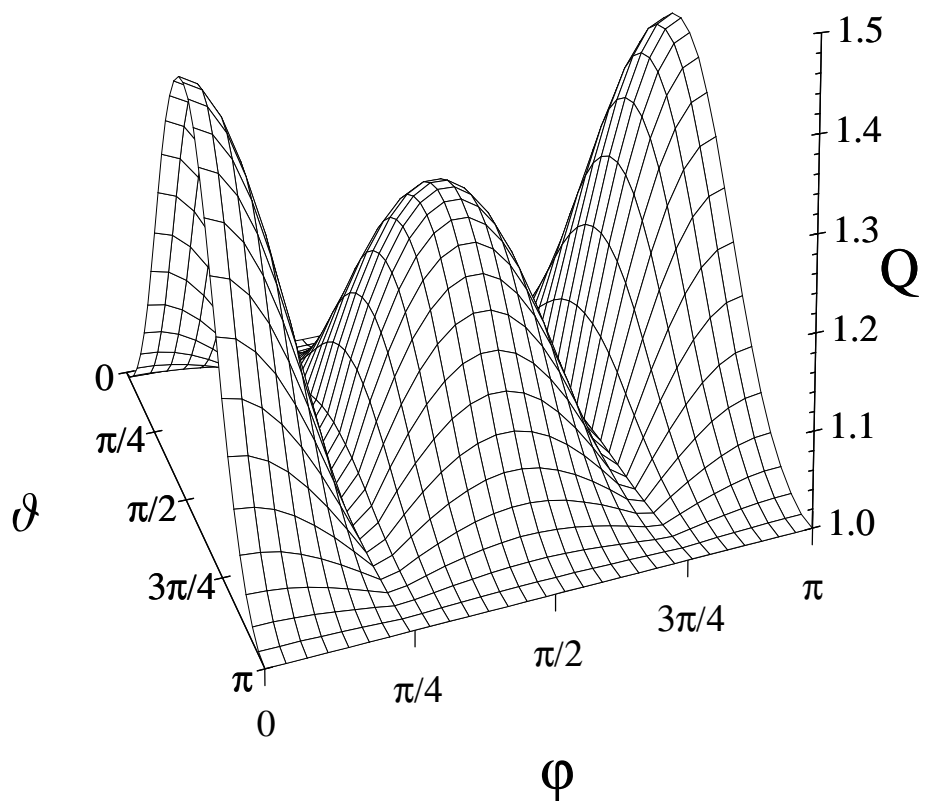
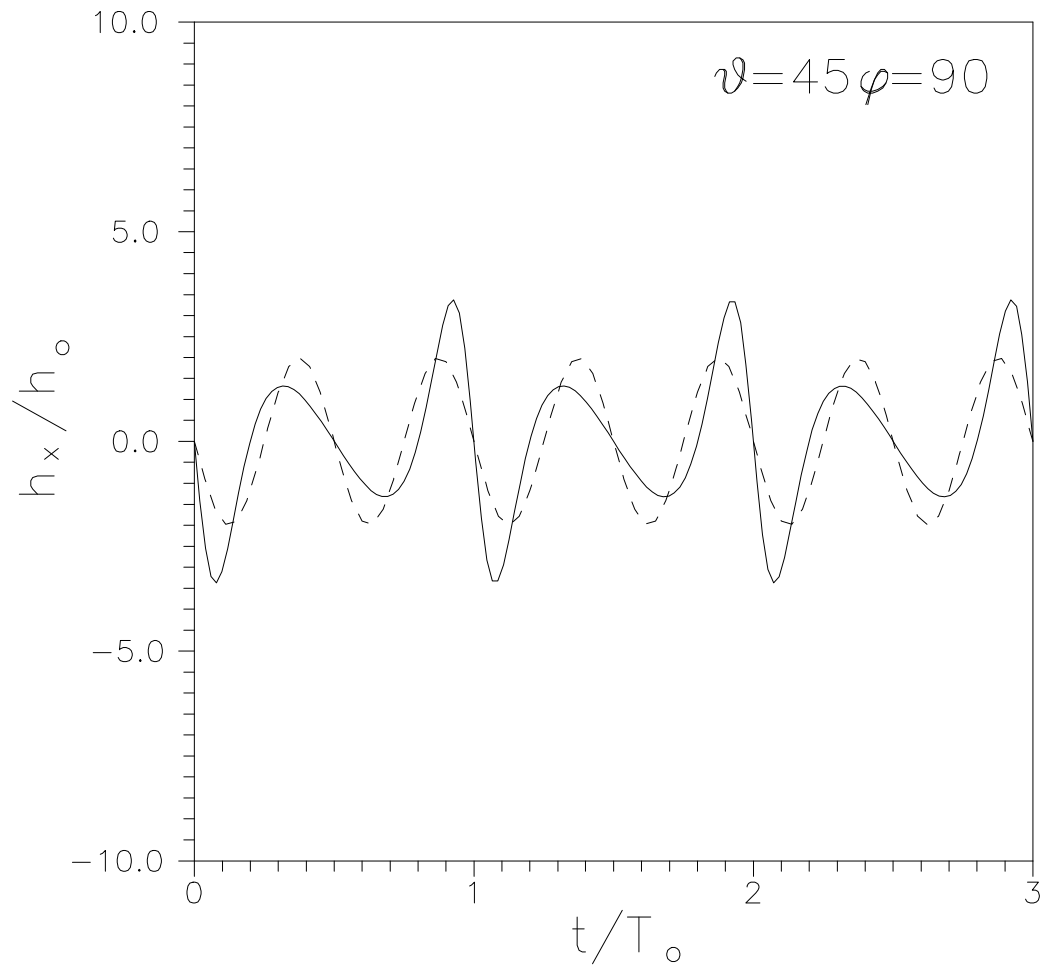
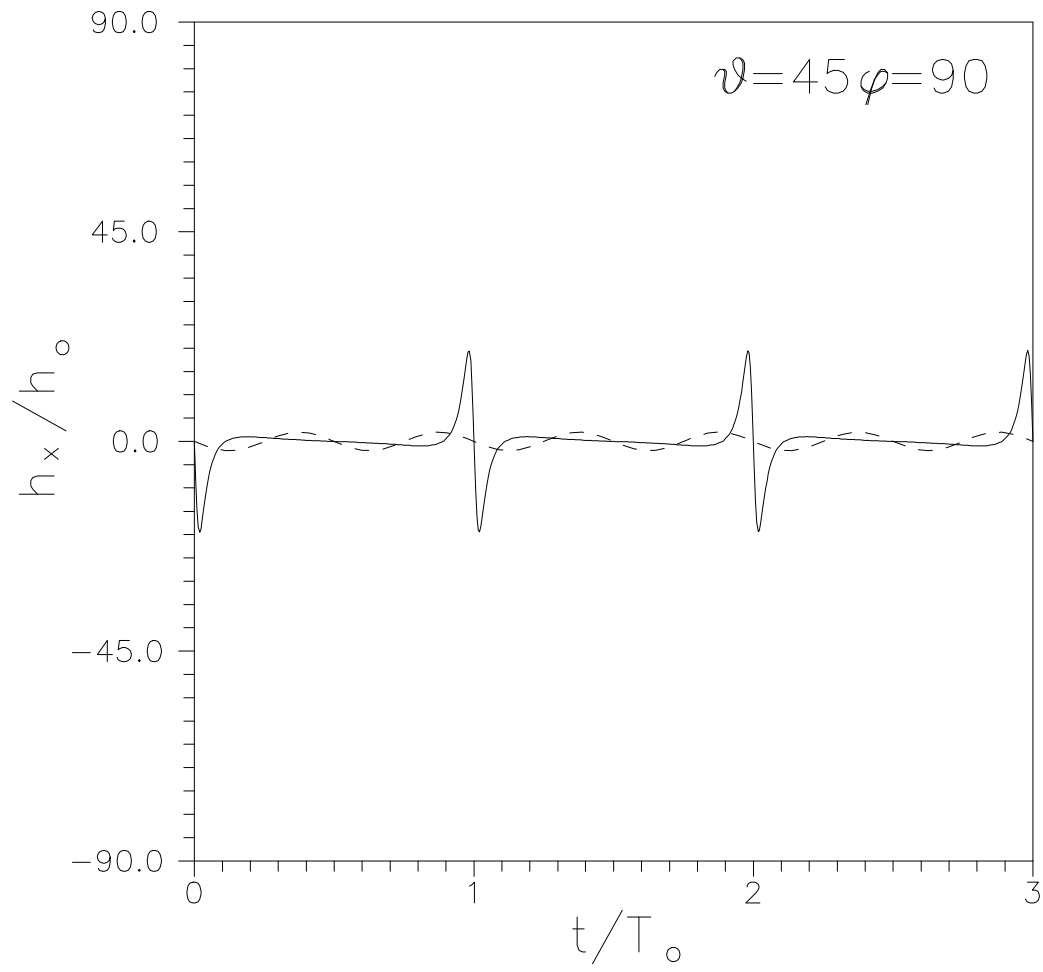


Fig 6 - The function  $Q(\vartheta, \varphi, e)$ , eq. (27).





*Fig. 7.6 - PSR1534+12 - a waveform gallery.*



*Fig. 8.6* - PSR1913+16 - a waveform gallery.

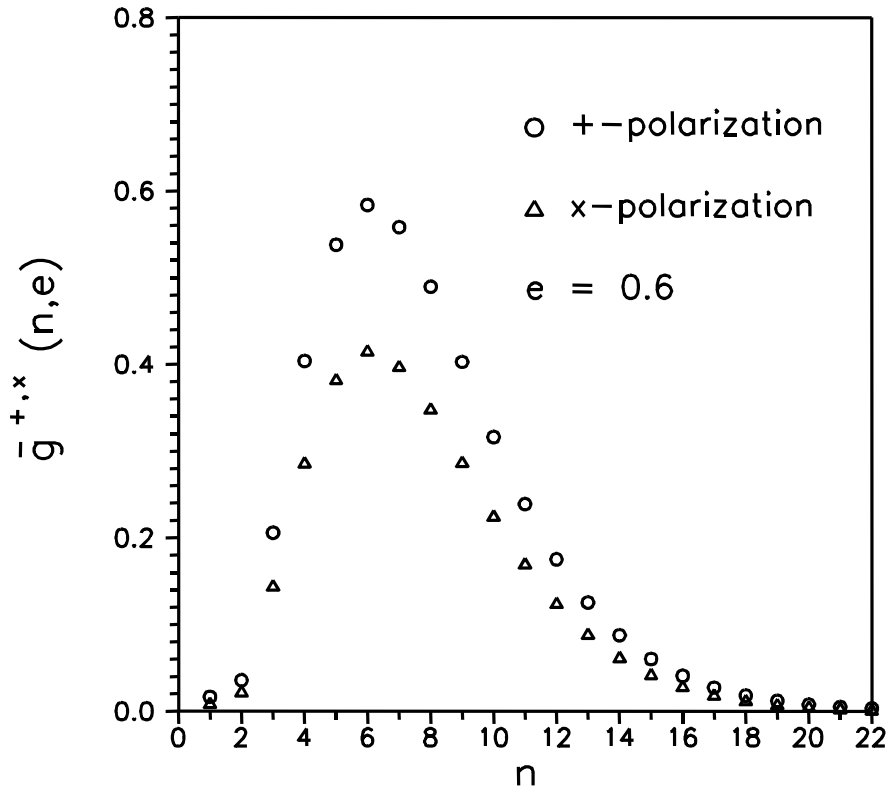
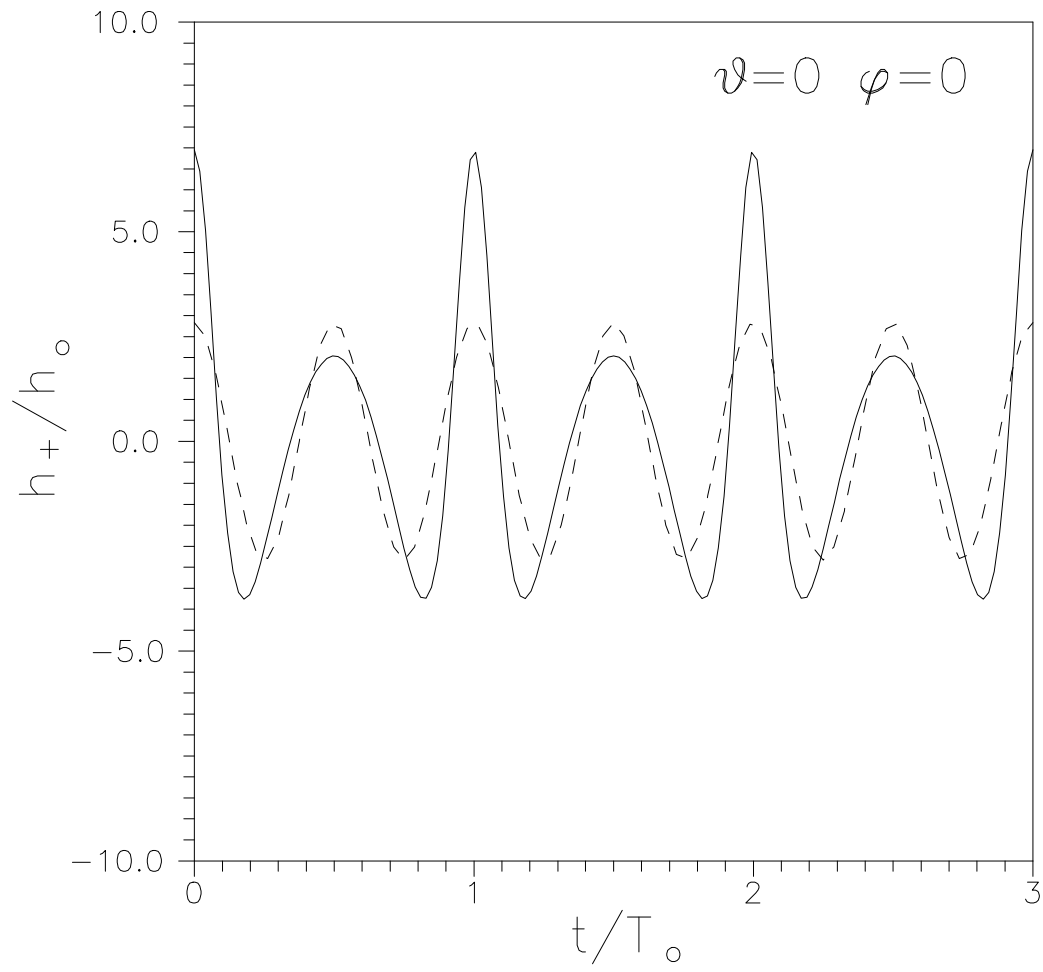
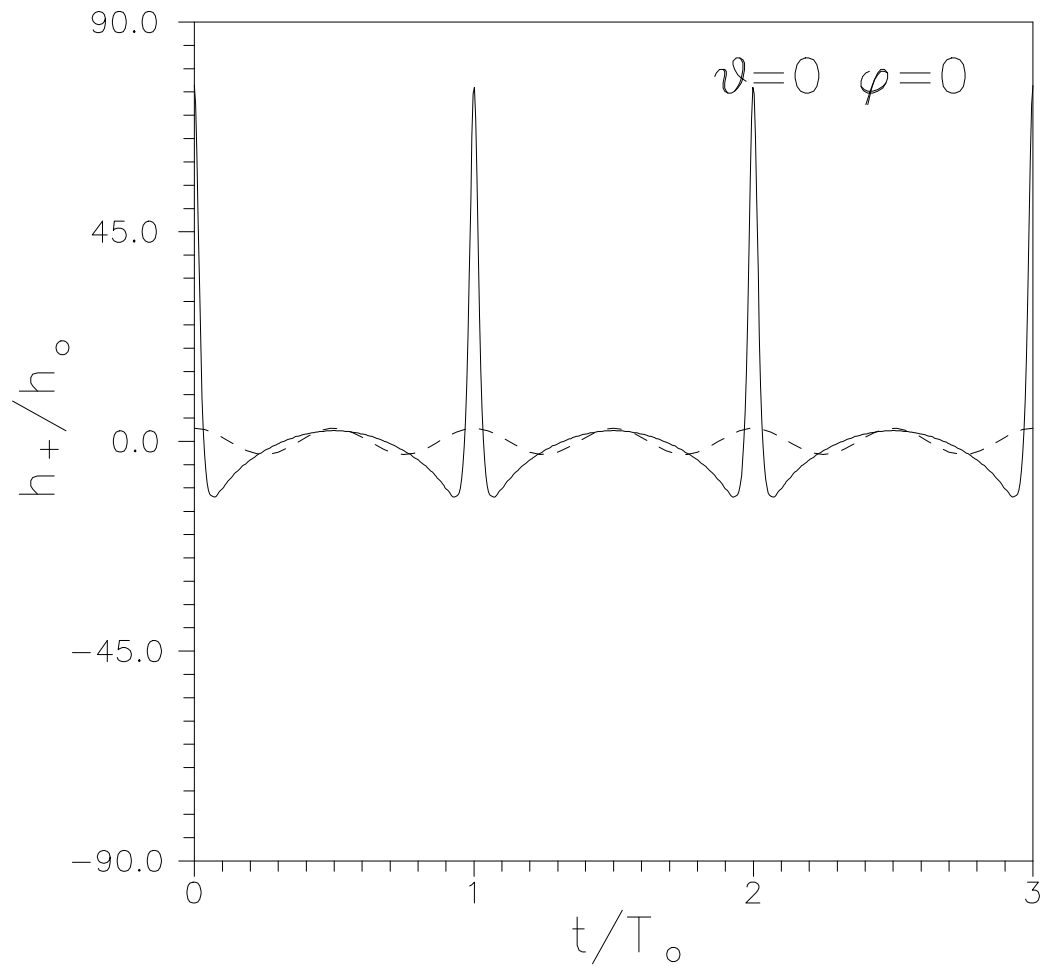


Fig. 1.7 -  $\bar{g}_{+,x}^{+,x}(n,0.6)$ , relevant to eq. (5).



*Fig. 7.7* - PSR1534+12 - a waveform gallery.



*Fig. 8.7* - PSR1913+16 - a waveform gallery.

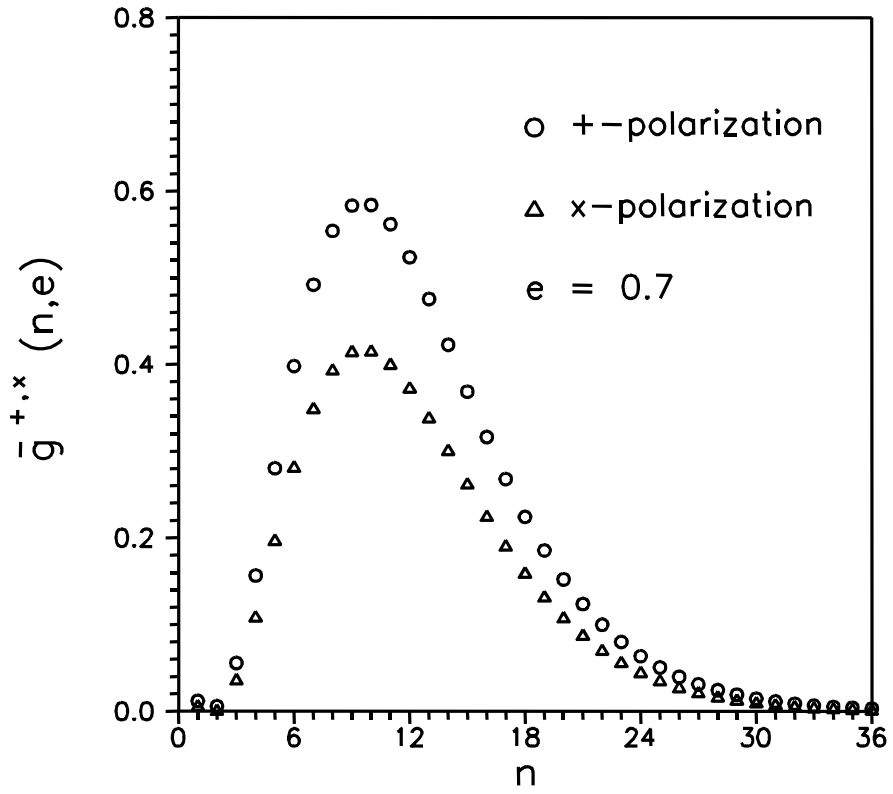
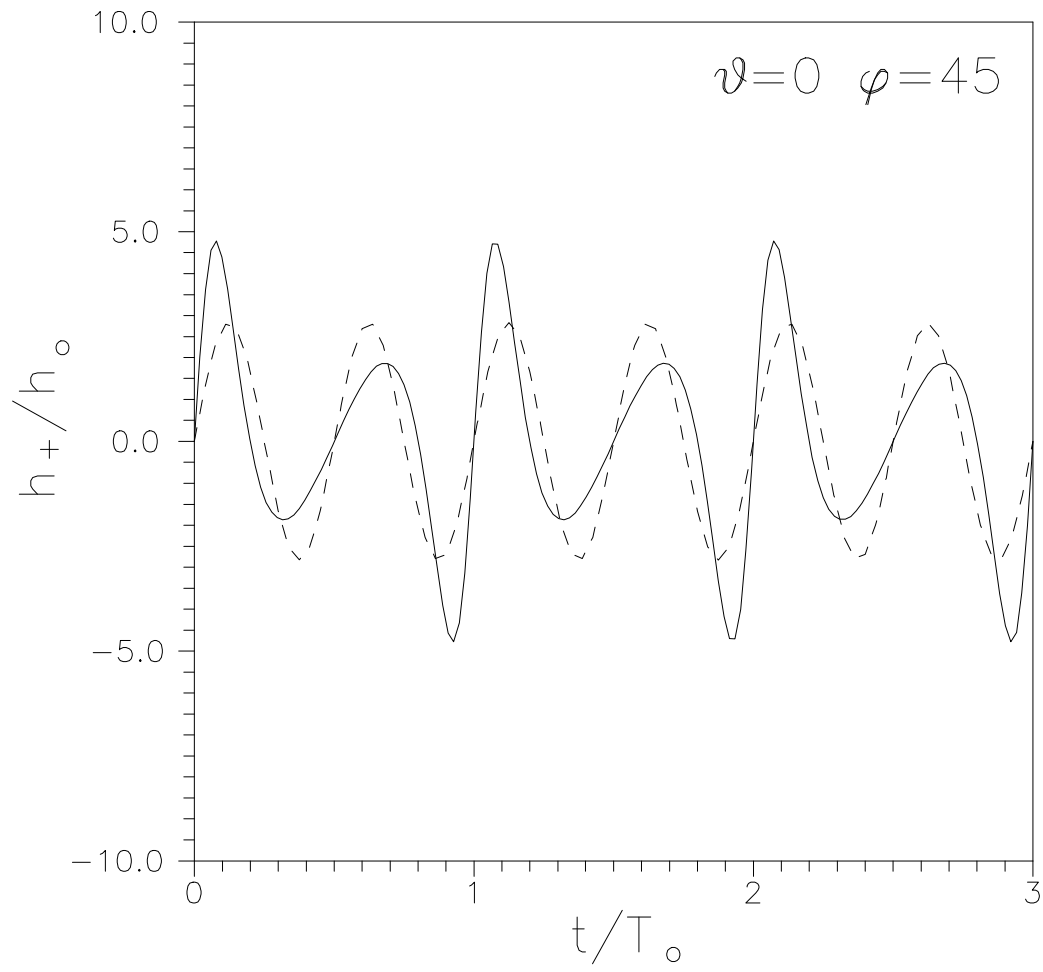
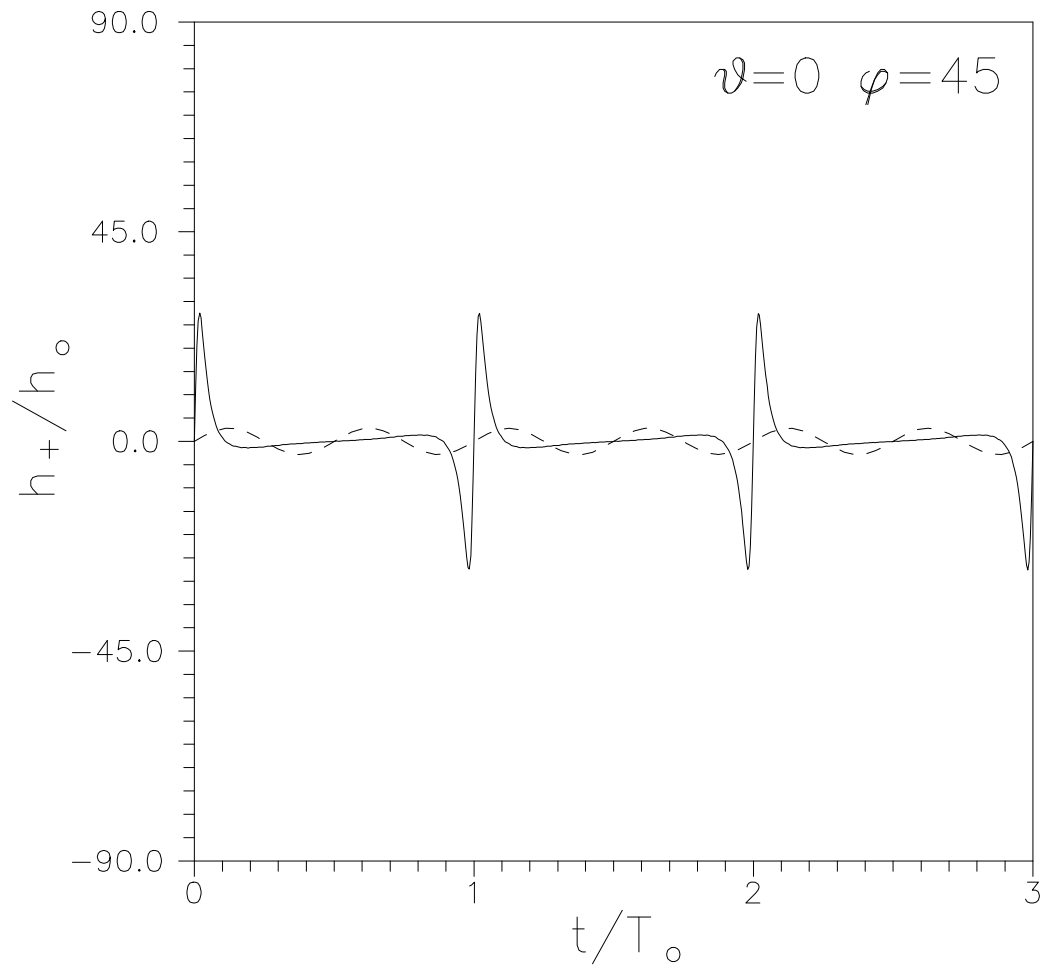


Fig. 1.8 -  $\bar{g}_{+,x} \cdot (n, 7)$ , relevant to eq. (5).



*Fig. 7.8* - PSR1534+12 - a waveform gallery.



*Fig. 8.8* - PSR1913+16 - a waveform gallery.



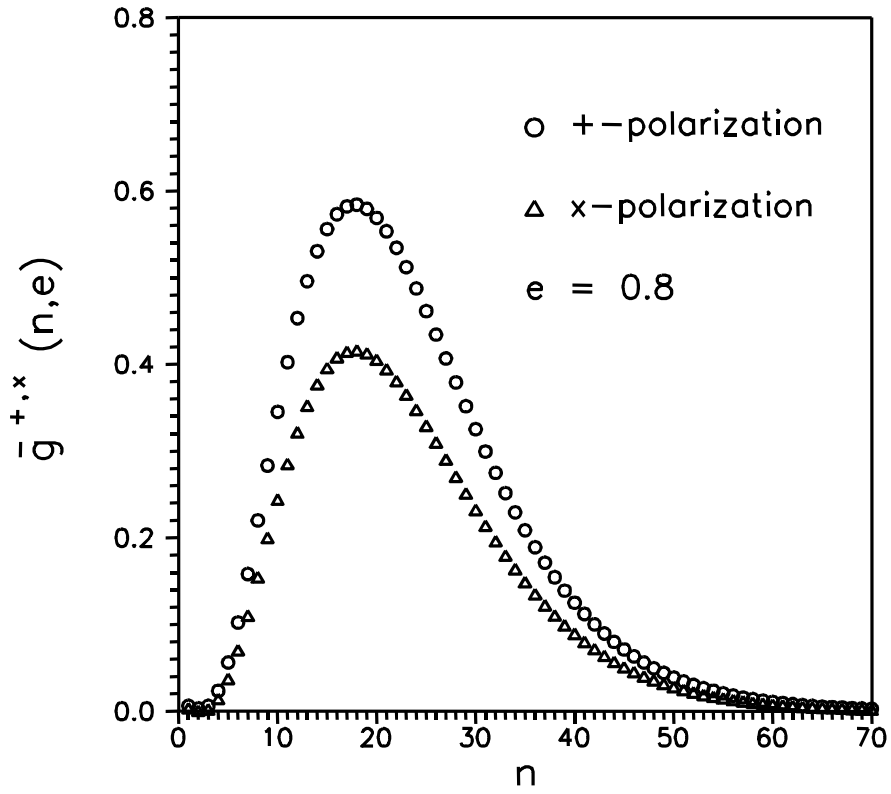
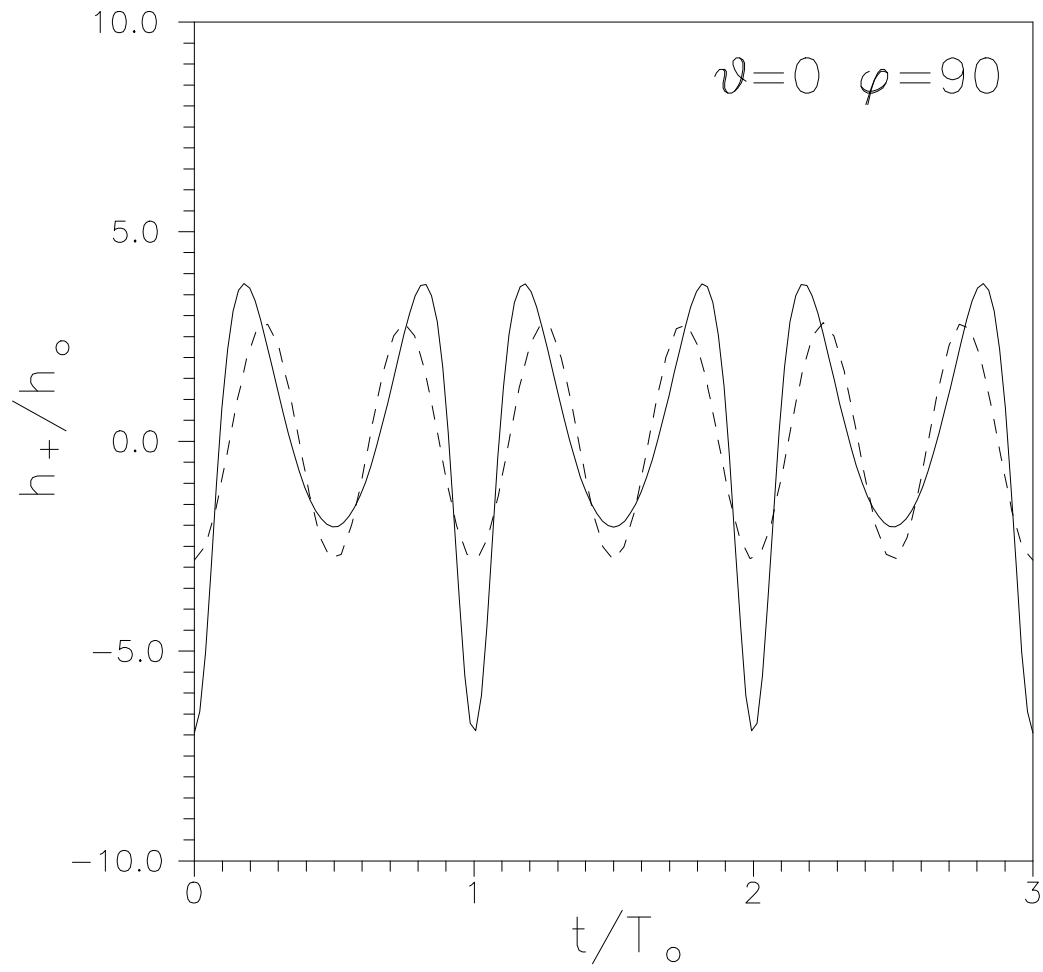
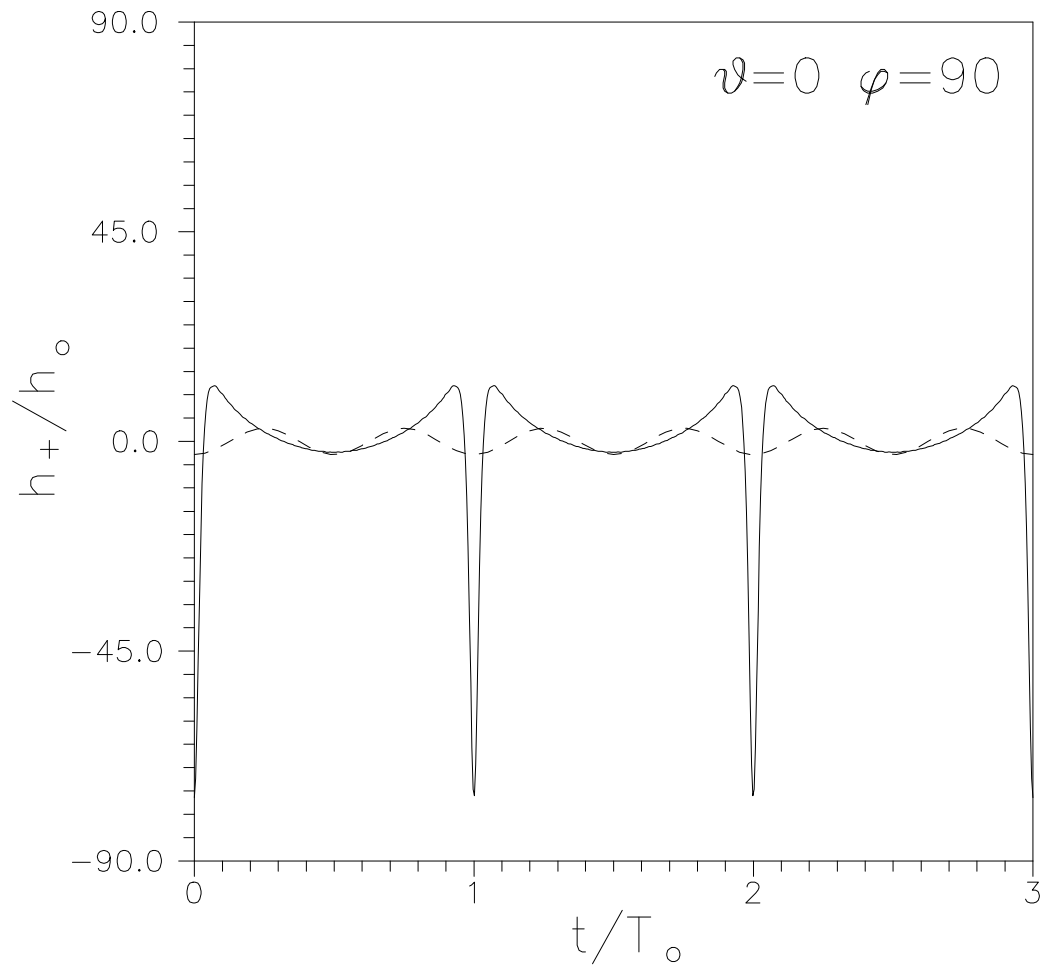


Fig. 1.9 -  $\bar{g}_{+,x}^{+}(n,0.8)$ , relevant to eq. (5).



*Fig. 7.9* - PSR1534+12 - a waveform gallery.



*Fig. 8.9* - PSR1913+16 - a waveform gallery.

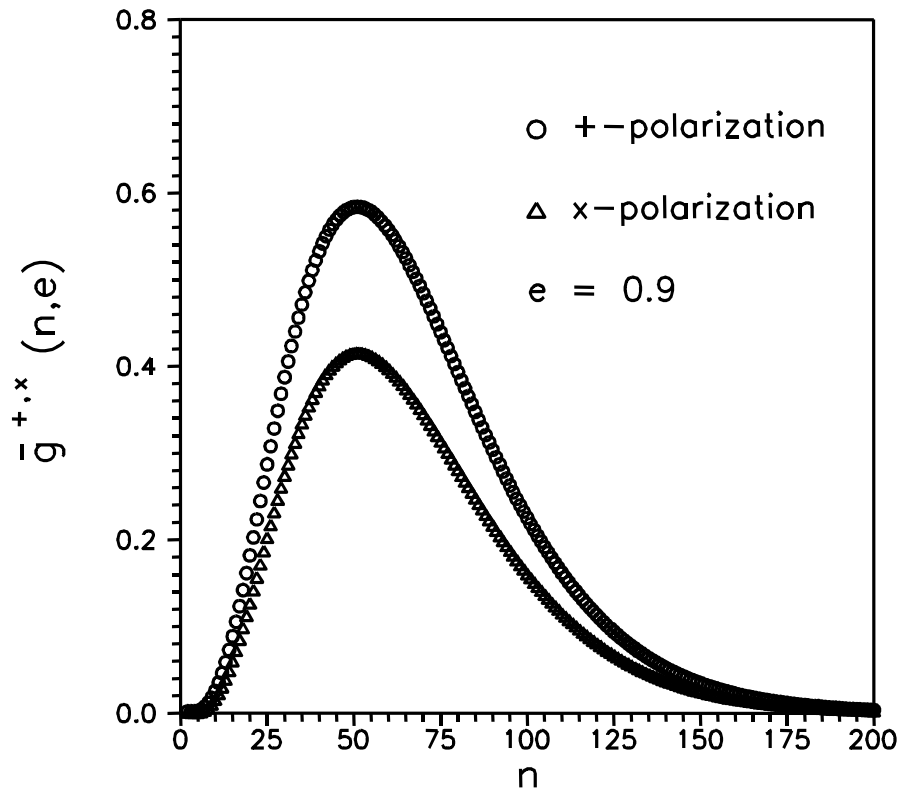
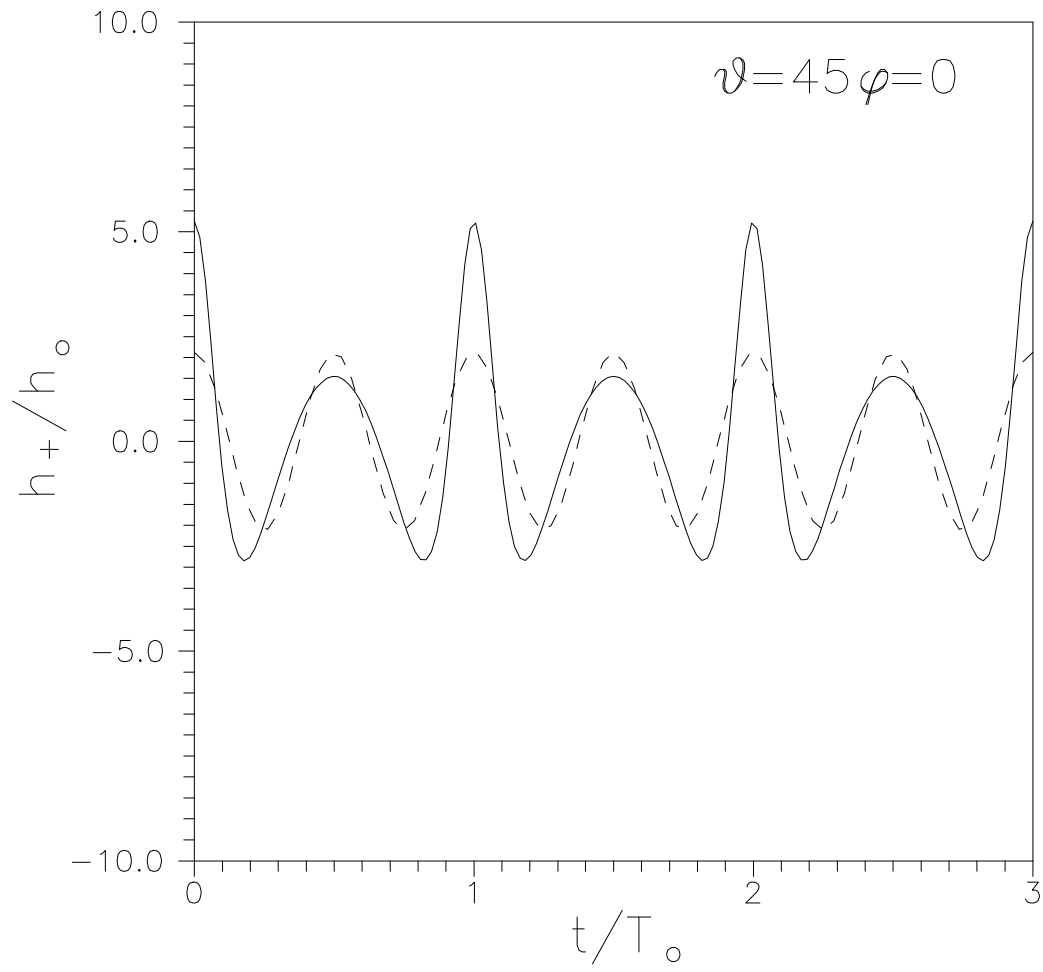
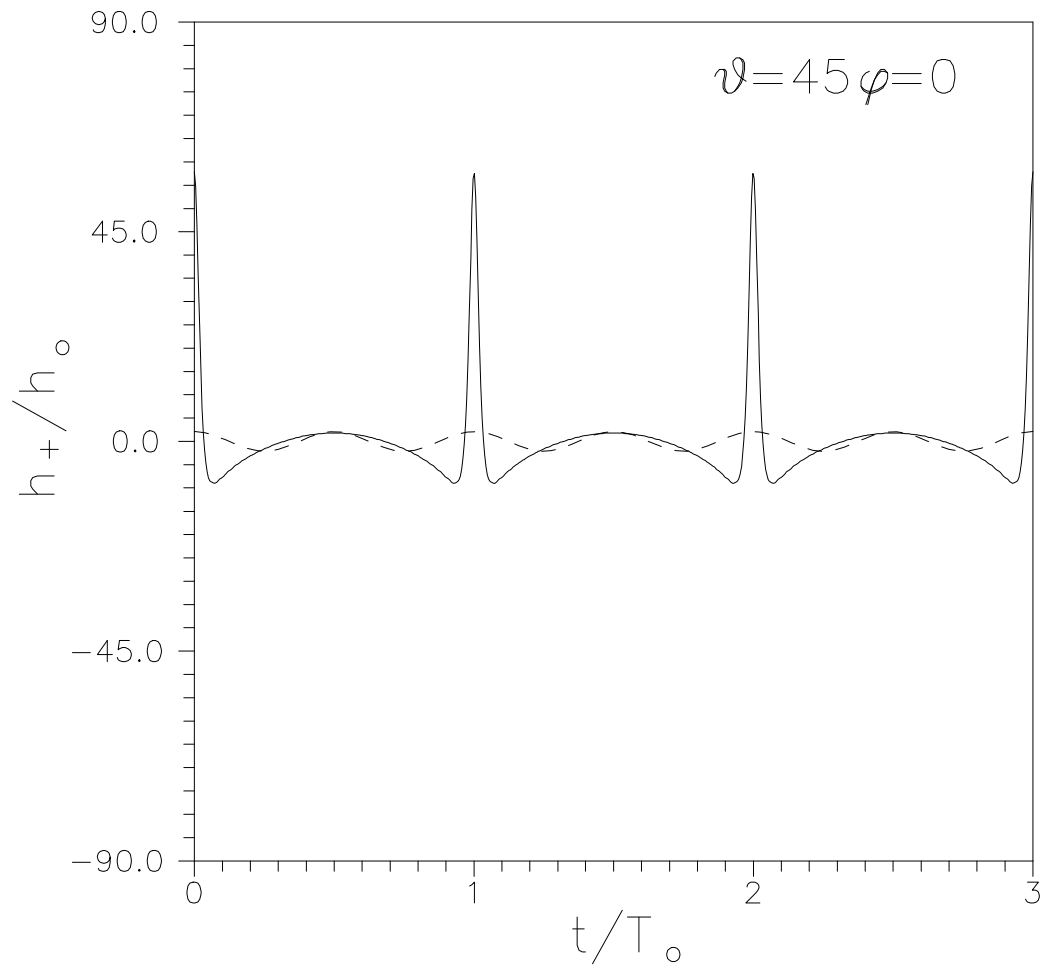


Fig. 1.10 -  $\bar{g}_{+,x}^{+}(n,0.9)$ , relevant to eq. (5).



*Fig. 7.10* - PSR1534+12 - a waveform gallery.



*Fig. 8.10* - PSR1913+16 - a waveform gallery.

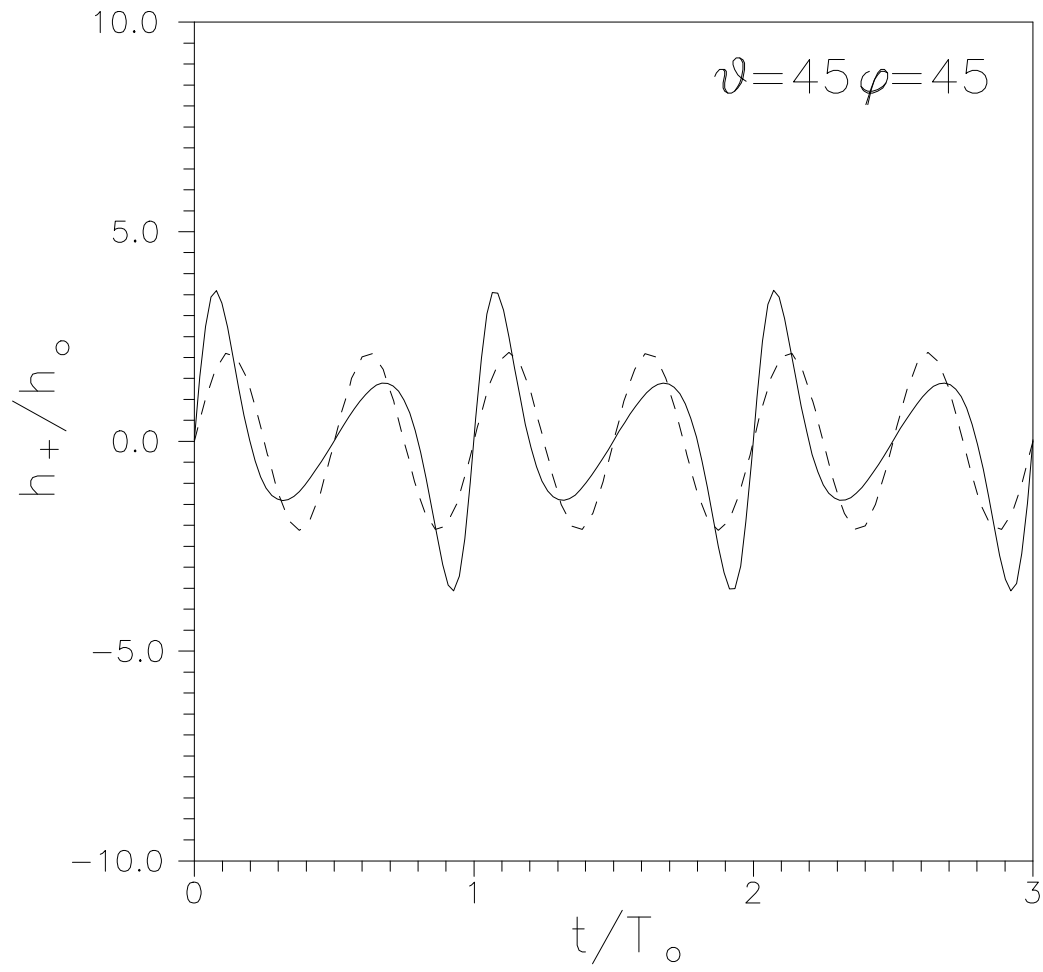


*Fig. 7.11* - PSR1534+12 - a waveform gallery.

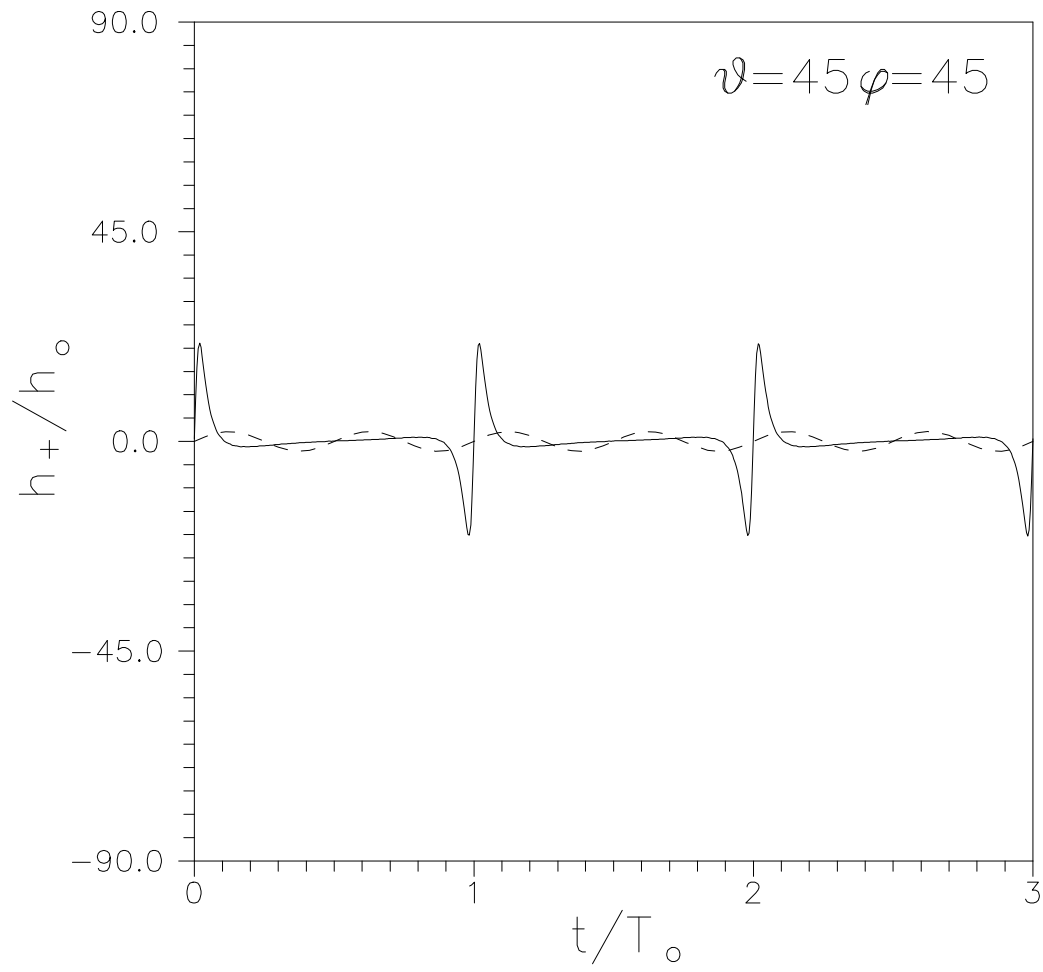


*Fig. 8.11* - PSR1913+16 - a waveform gallery.



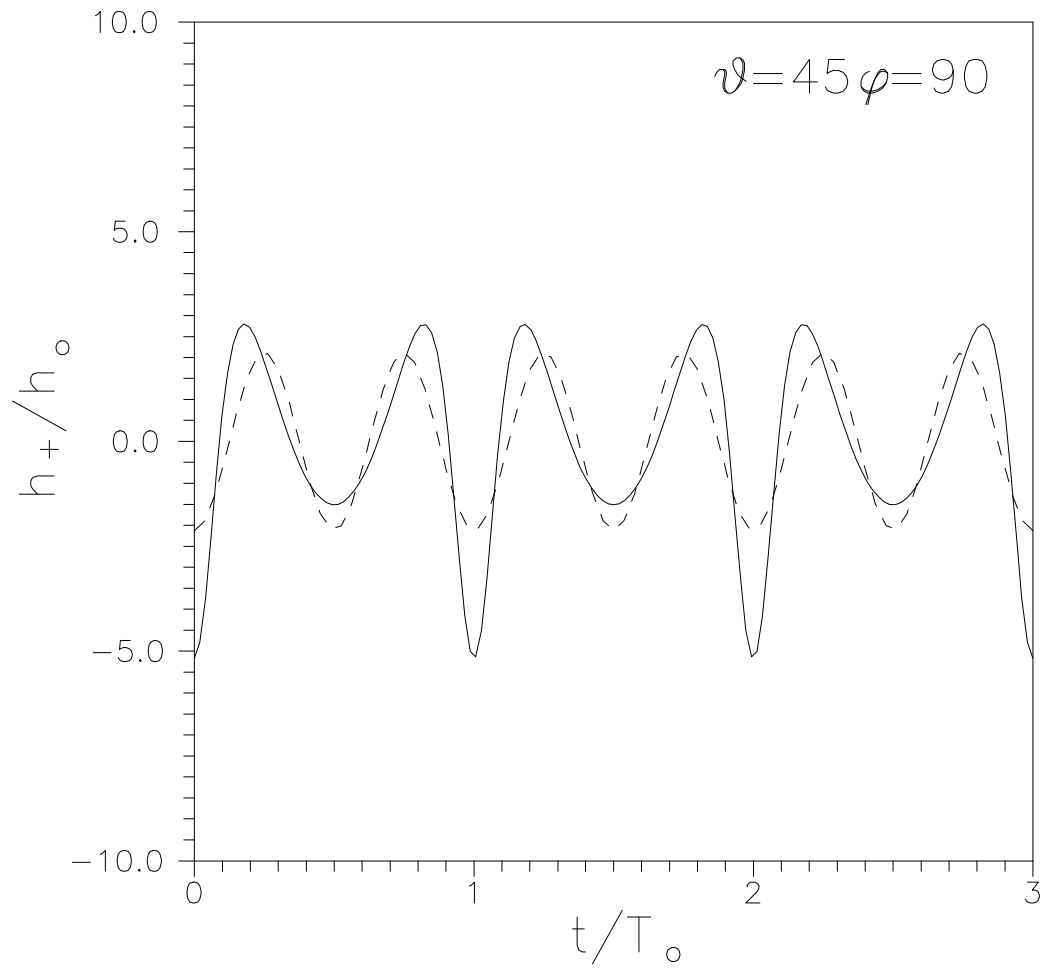


*Fig. 7.12* - PSR1534+12 - a waveform gallery.

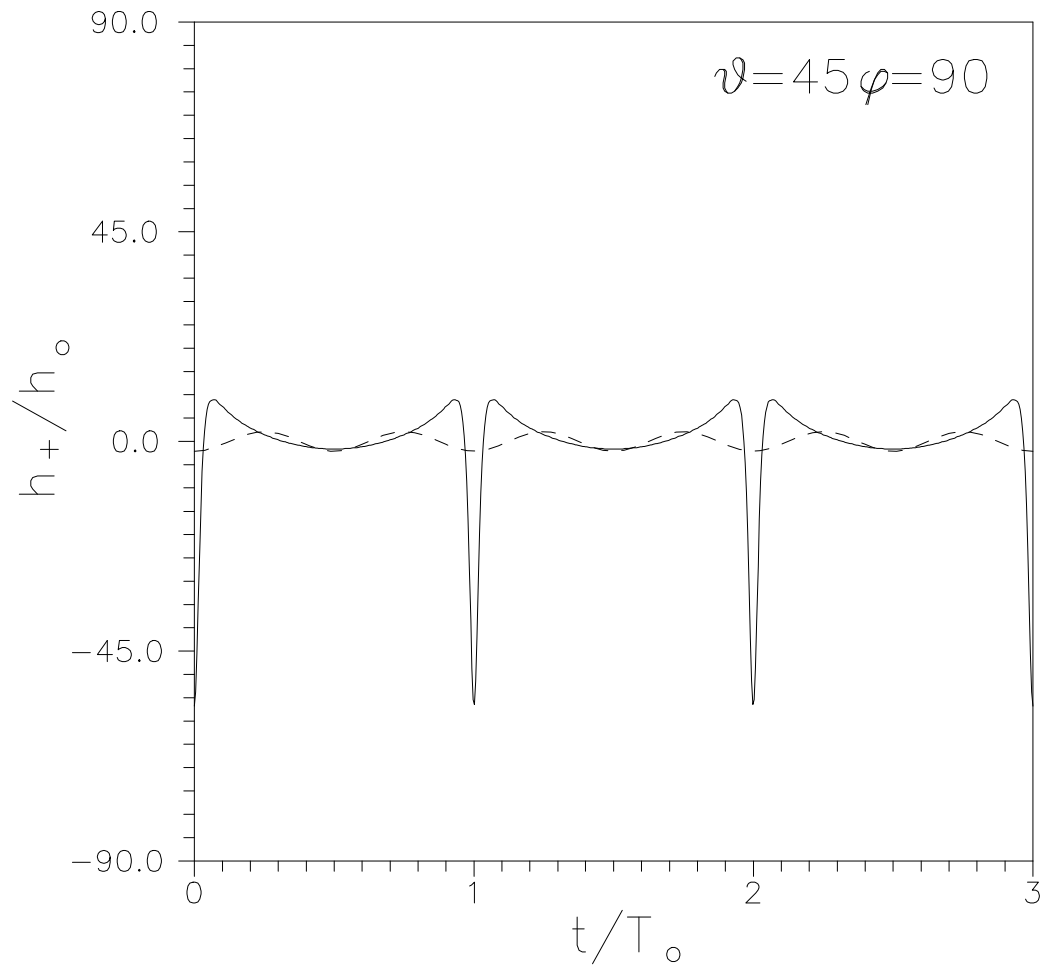


*Fig. 8.12* - PSR1913+16 - a waveform gallery.

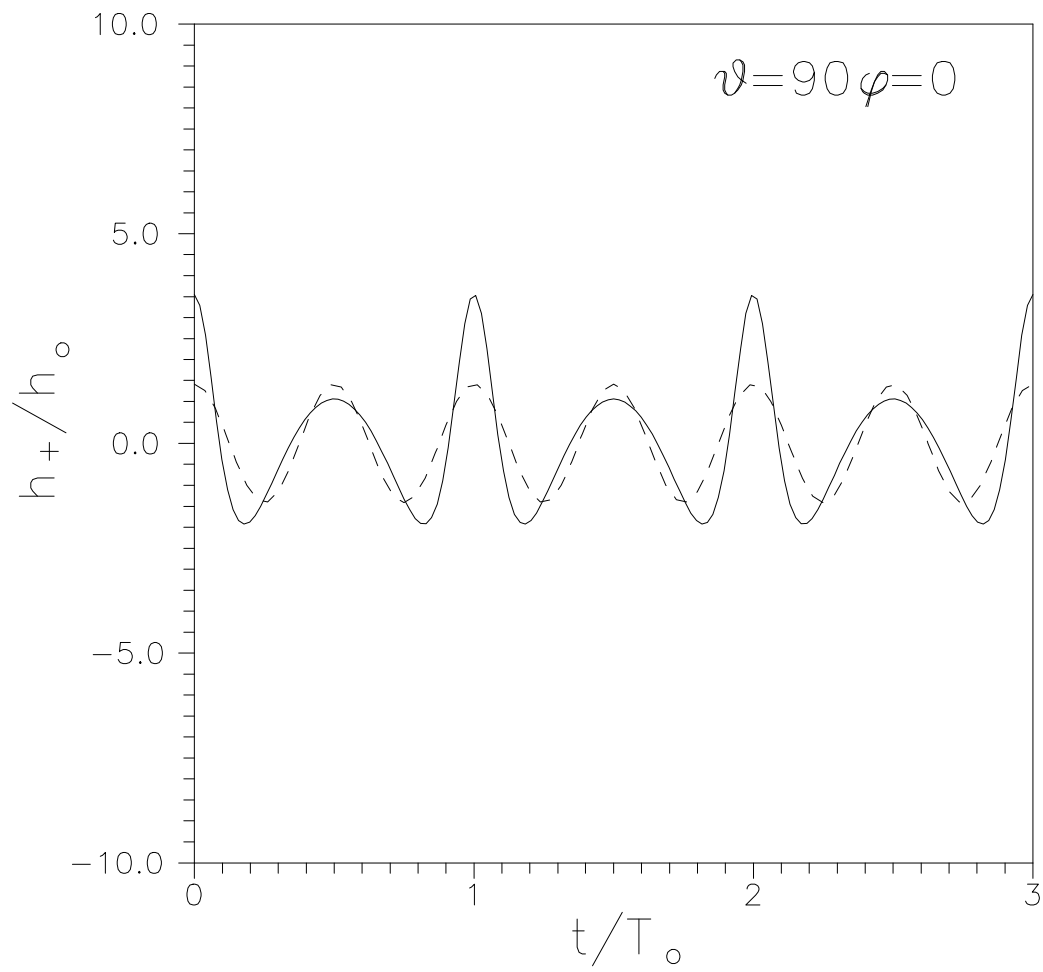


*Fig. 7.13* - PSR1534+12 - a waveform gallery.

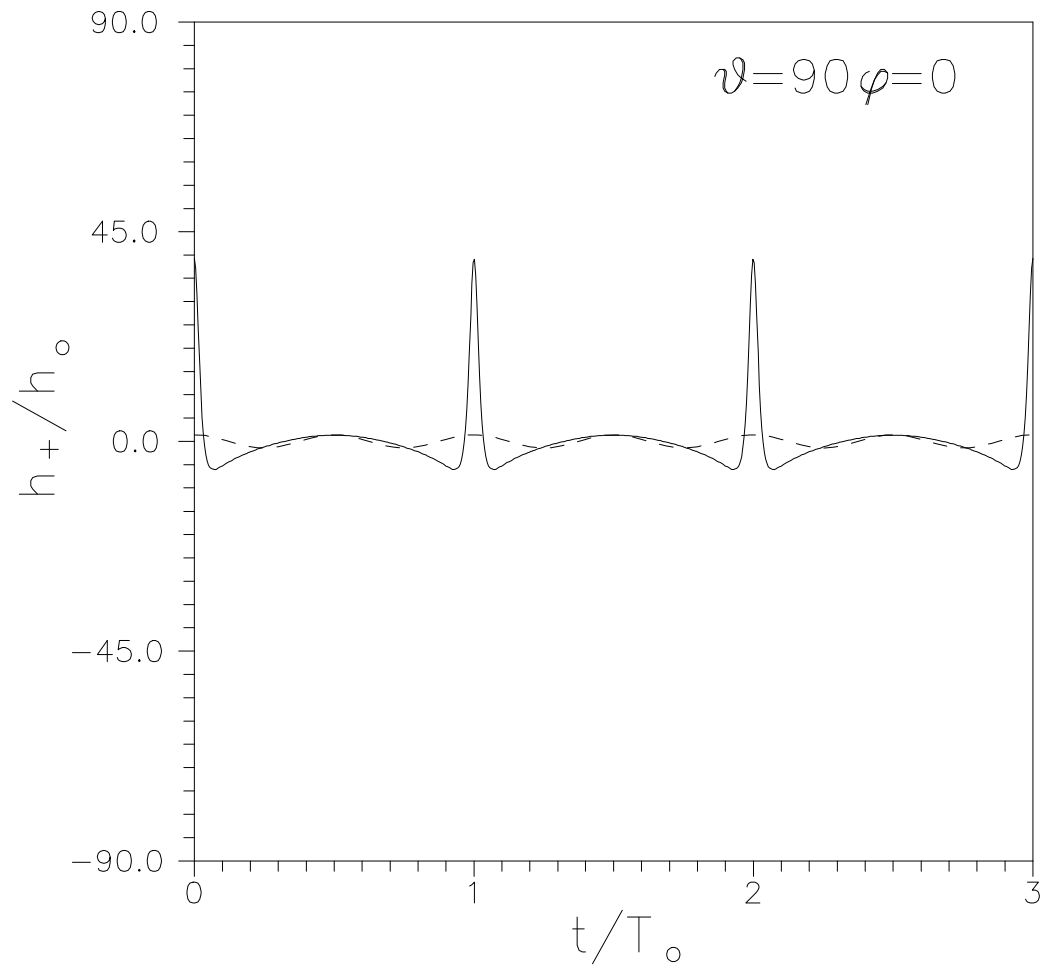


*Fig. 8.13* - PSR1913+16 - a waveform gallery.

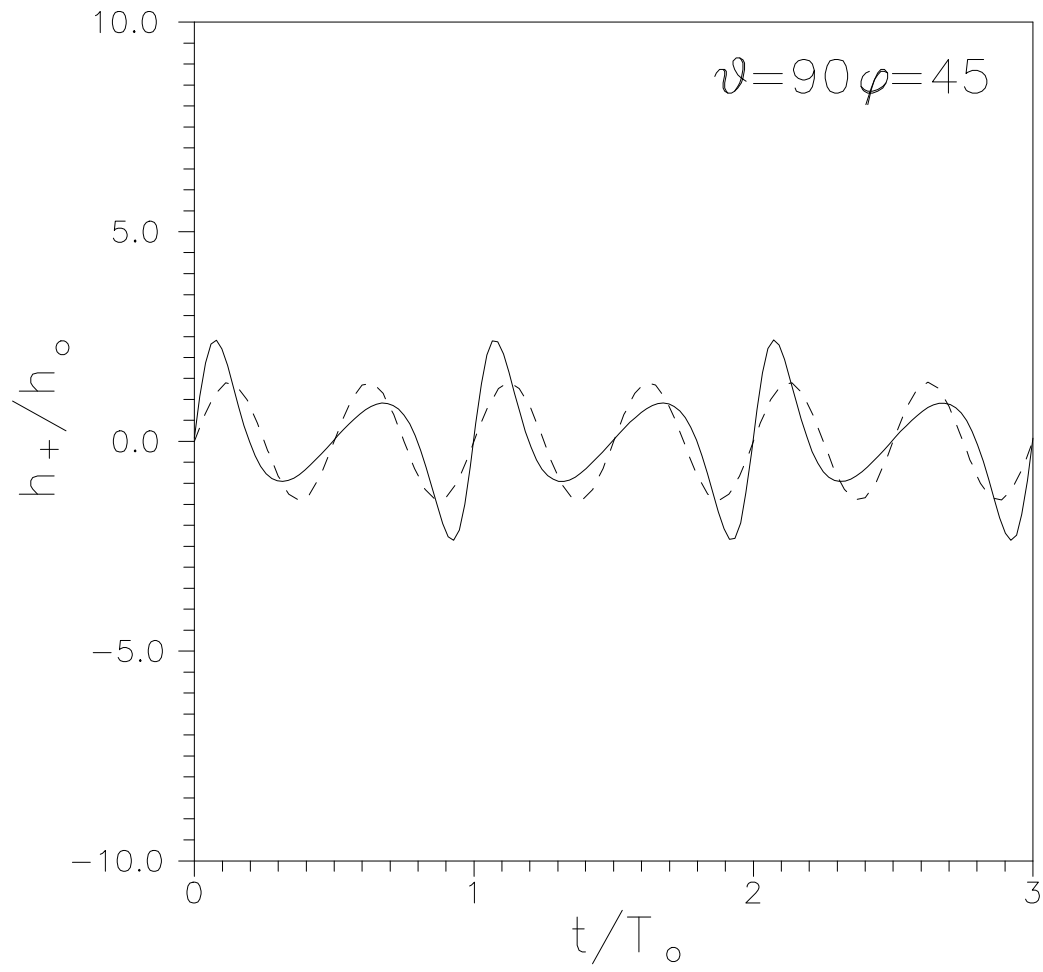


*Fig. 7.14* - PSR1534+12 - a waveform gallery.

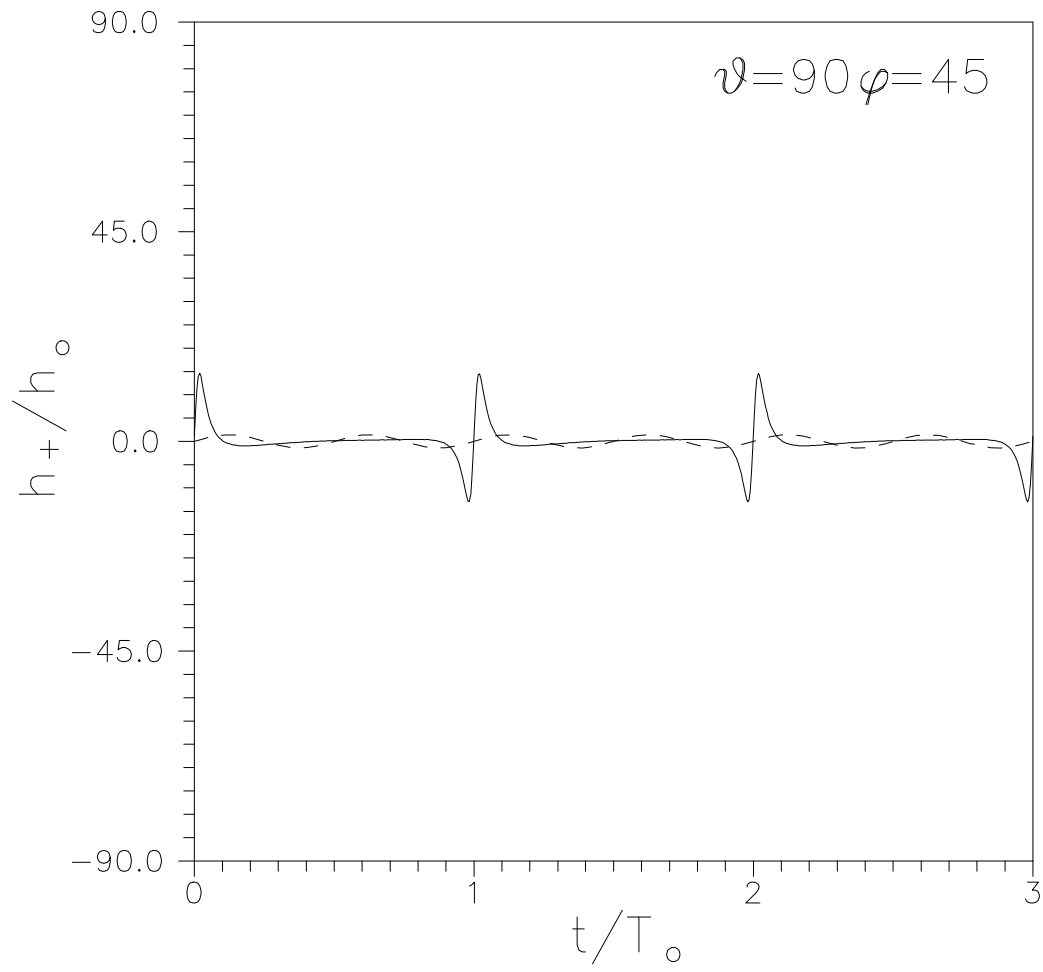


*Fig. 8.14* - PSR1913+16 - a waveform gallery.

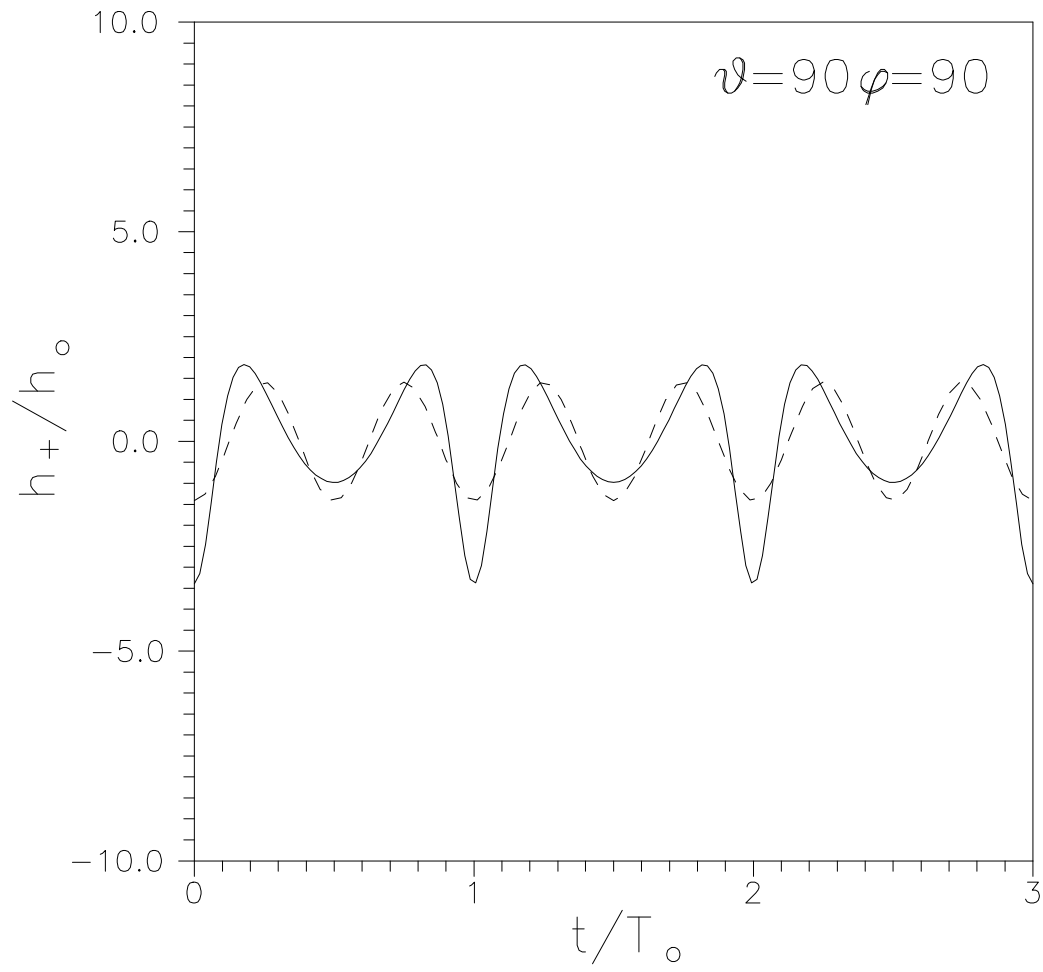


*Fig. 7.15* - PSR1534+12 - a waveform gallery.

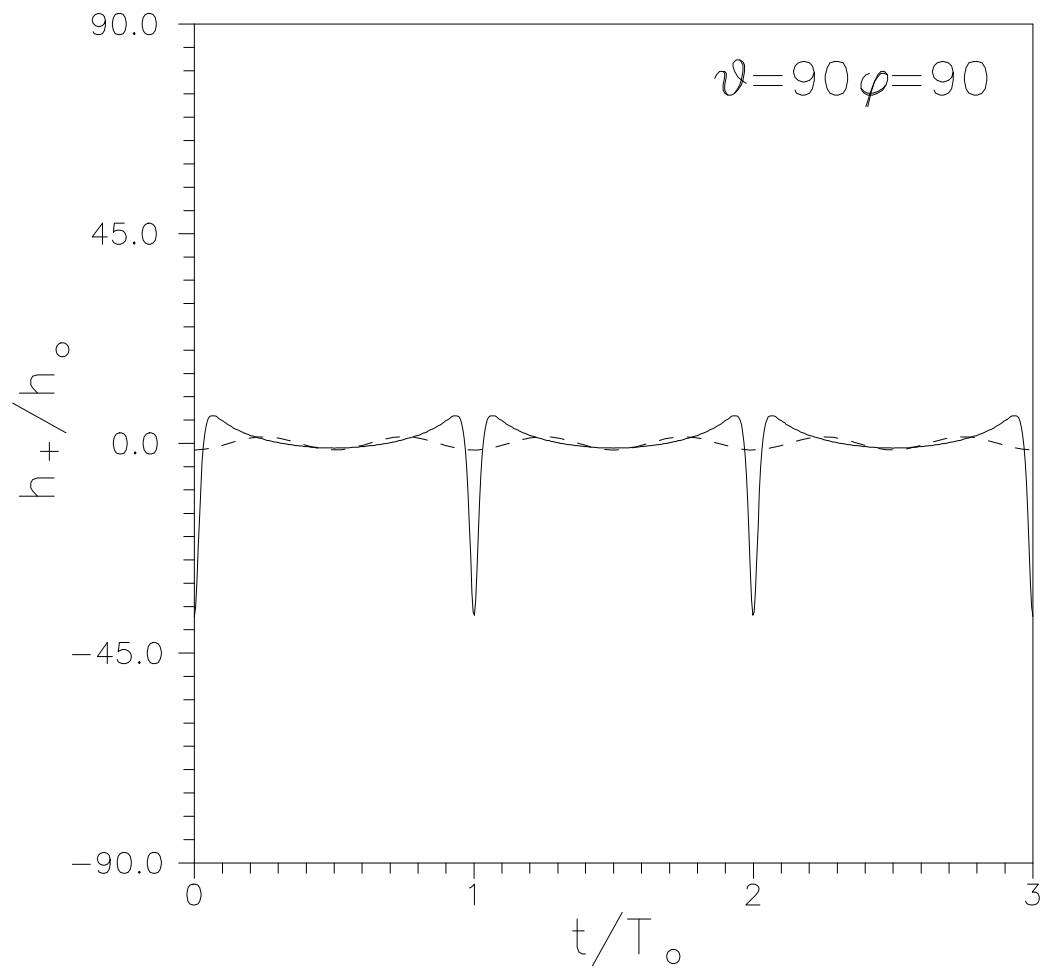


*Fig. 8.15* - PSR1913+16 - a waveform gallery.